J. Fluid Mech. (1997), *vol.* 331, *pp.* 373–403

Copyright © 1997 Cambridge University Press

The thin liquid lining of a weakly curved cylindrical tube

By O. E. JENSEN

Department of Applied Mathematics and Theoretical Physics,
University of Cambridge, Silver Street, Cambridge CB3 9EW, UK

(Received 1 April 1996 and in revised form 18 July 1996)

A thin-film approximation is used to study the effects of surface tension on a thin liquid layer lining the interior of a cylindrical tube, where the tube has radius a and a centreline with weak, uniform curvature δ/a. Centreline curvature induces a pressure gradient in the fluid layer, analogous to that due to a weak gravitational field, that drives fluid from the inner to the outer wall of the tube, i.e. away from the centre of centreline curvature. The resulting draining flow is computed numerically under the assumption of axial uniformity, and the large-time asymptotic draining regimes and flow structures are identified. In the absence of destabilizing intermolecular interactions, the inner wall remains wet, covered with a vanishingly thin fluid layer, while a near-equilibrium lobe forms on the outer wall. The stability of this quasi-static lobe to axial variations is then investigated by using numerical and perturbation methods to solve the linearized Young–Laplace equation, prescribing zero contact angle at the lobe's free boundary. Conditions on δ, the fluid volume a^3V and the tube length aL are identified separating axially uniform lobes (which are stable for low $V/(\delta L)$ or small L), wavy lobes (some with a solitary structure) and localized fluid droplets (which exist for sufficiently large V/δ and L). Hysteresis is demonstrated between multiple equilibria, the topology of which can change dramatically as parameters are varied. The application of these results to lung airways is discussed.

1. Introduction

The airways of the lung constitute a network of bifurcating, flexible tubes that are lined on their interior with a thin, surfactant-covered liquid layer. The distribution of this fluid lining, particularly in the smaller airways, is strongly influenced by surface tension. Since a sufficiently long, cylindrical, air–liquid interface is unstable to axial, surface-tension-driven perturbations (Plateau 1873; Rayleigh 1879), an initially uniform liquid lining on the interior of a straight cylindrical tube may form either axisymmetric wetting collars around the wall or, if there is a sufficient volume of fluid available, a liquid bridge across the tube (Goren 1962; Everett & Haynes 1972; Hammond 1983; Gauglitz & Radke 1988; Johnson *et al.* 1991; Newhouse & Pozrikidis 1992). Gas exchange is impaired if an airway is occluded by such an instability, making 'airway closure' of major importance in respiratory mechanics (e.g. Macklem, Proctor & Hogg 1970; Kamm & Schroter 1989; Grotberg 1994). These capillary instabilities are also of importance in two-phase porous-media flows, such as those associated with oil recovery (e.g. Olbricht 1996).

Each lung airway is relatively short, and forms part of a bifurcation at each of its ends, so that over substantial portions of its length the curvature of the airway

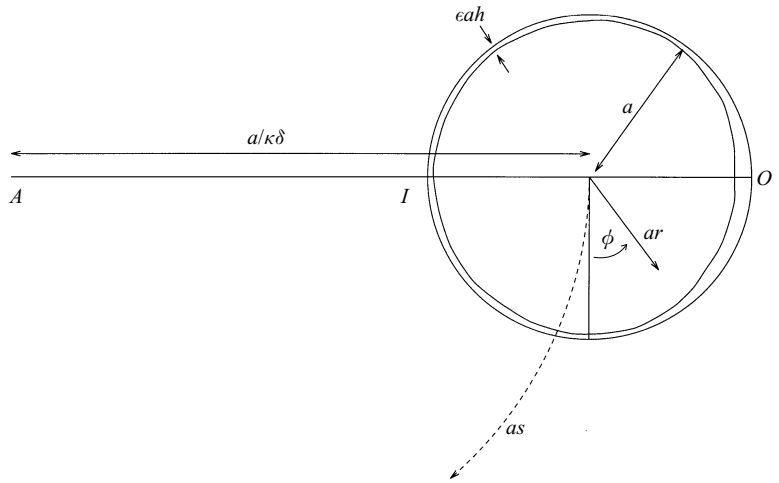

FIGURE 1. A thin film lines the interior of a curved tube. A denotes the centre of centreline curvature; I [O] denotes that half of the interior wall closer to [further from] A, i.e. the inner [outer] wall of the bend in the tube.

wall is non-uniform. The thin liquid lining of an airway is therefore subject to surface-tension-generated pressure gradients associated, in particular, with gradients in wall curvature. It is important to understand the consequent draining flows and the stability of the resulting fluid distribution, since this will have important implications for the overall distribution of the airway liquid lining, for its capacity to protect the airway epithelium and for the dynamics of surfactant transport in airways. Similar draining flows can arise in porous-media applications, in small-scale manufacturing equipment and are of potential interest in the microgravity environment.

These considerations motivate a simple model problem in which a uniform tube with cylindrical cross-section and a weakly curved centreline is lined on its interior with a thin layer of Newtonian fluid. (The results carry over directly to the thin exterior lining of a curved cylinder, although this application is not pursued here.) The total wall curvature is greater on the outer wall of the tube than on the inner wall (where 'outer' denotes the interior wall further from the centre of centreline curvature, labelled O in figure 1). An initially uniform liquid lining, such as that deposited behind the nose of a semi-infinite bubble moving slowly down a liquid-filled tube, is unstable because the larger curvature at the outer wall generates a lower pressure in the fluid relative to that on the inner wall; the pressure gradient will drive fluid from the inner to the outer wall. In the thin-film, weak-curvature limit, this pressure gradient turns out to be equivalent to that due to a weak gravitational field acting on the thin lining of a straight tube with its axis horizontal, a configuraton examined recently by Reisfeld & Bankoff (1992). The dynamics of the resulting draining flow can be modelled using lubrication theory, by incorporating the leading-order effects of centreline curvature in an evolution equation for the film thickness.

Computations presented below of this axially uniform, azimuthal draining flow reveal that it has a large-time asymptotic structure that is typical of draining problems in which 'dimples' are created at deformable interfaces, such as during the buoyancy-driven motion of a nearly spherical bubble through a fluid interface (Jones & Wilson 1978), the draining of a squeeze film between a cell membrane and a rigid or stress-free surface (Wu & Weinbaum 1982), the formation of axisymmetric wetting collars

in thin films lining straight cylindrical tubes (Hammond 1983) and the draining of a fluid droplet under gravity on a vertical wall (Tuck & Schwartz 1991). There is a flux of fluid, that diminishes with time, from an emptying lobe on the inner wall, in which the film thickness falls rapidly, into a relatively large, near-equilibrium lobe on the outer wall. These two regions are connected by a short transition region in which the film is locally extremely thin. The increased resistance to flow in this thin region allows draining to persist indefinitely, in the absence of intermolecular forces. These forces would either cause the film to rupture at its thinnest point (if they were destabilizing) or ultimately halt the drainage (if they were stabilizing); these possibilities were considered by Reisfeld & Bankoff (1992), but such effects are not explicitly included in the present model. It is shown instead that for a liquid lining that wets the tube wall, there are generally two distinct draining regimes at large times: a transient phase in which the flux is $O(t^{-5/4})$ at time t; and a later phase in which the flux is $O(t^{-3/2})$, the inner-wall lobe drains unsteadily and a capillary wave train with a complex asymptotic structure forms upstream of the thinnest part of the film. The main purpose of this calculation is to show that at very large times the solution is well approximated by the quasi-static outer-wall lobe alone (i.e. by the 'outer' solution in the language of matched asymptotic expansions); at its boundary (the transition region), the lobe has zero contact angle at an effective contact line; the drained region on the inner wall can be treated as effectively dry.

The stability of this equilibrium lobe to axial variations is then considered. A uniform lobe, which resembles a static rivulet (see, for example, Davis 1980; Langbein 1990), is shown to be linearly unstable to long-wavelength axial perturbations if the effective contact lines lie in the inner half of the tube; the lobe is linearly stable if it is confined entirely to the outer wall. The boundary of neutral stability is presented in terms of the fluid volume a^3V (where a is the tube radius), the tube length (or solution period) aL and the centreline curvature δ/a. This reveals the stabilizing effect of centreline curvature: whereas for a straight tube the axially uniform equilibrium state is unstable for all V provided L is sufficiently large (i.e. for $L > 2\pi$), for a curved tube there is a critical value of V/δ below which axial uniformity is guaranteed for all L.

Liquid-lining flows are driven by competing viscous and capillary forces such that the system moves dissipatively down gradients of free energy, i.e. gradients of effective surface area (Everett & Haynes 1972). By identifying all energy extrema (i.e. all possible equilibria), the bifurcation structure of the static solutions can be used to infer their local stability (Michael 1981; Ungar & Brown 1982), yielding a picture of the overall dynamics of the system. Thus to take the study of lobe stability further, we investigate all possible equilibrium solutions of the Young–Laplace equation (here in its linearized, thin-film formulation it is a forced Helmholtz equation) using L and V/δ as independent bifurcation parameters. This is a nonlinear, free boundary problem because the location of the contact lines (at which there is zero contact angle) must be determined as part of the solution. Similar calculations of capillary equilibria with free contact lines have been performed by Higgins & Brown (1984), Sáez & Carbonell (1987), Langbein (1990) and others. A weakly nonlinear analysis shows that an axially uniform lobe bifurcates either supercritically or subcritically to a branch of wavy lobes, depending on the tube length. Solution branches are then extended numerically to finite amplitudes. It is shown how there can be hysteresis in the transition between axially uniform and wavy solutions. Further, in long tubes the wavy solutions can assume a solitary asymptotic structure, whereby a fluid blob is connected to a thin axially uniform strip of fluid. For V/δ greater than a critical

value, the thin strips vanish and the blobs become isolated, forming localized droplets on the outer wall of the tube; these droplets are analogues of the localized stable wetting collars that exist in straight tubes.

The model is outlined and axially uniform equilibrium states are discussed in §2. The axially uniform draining flow is computed in §3. The stability problem is treated analytically in §4 and numerically in §5. Some implications of the results are discussed in §6.

2. The model

We derive here the leading-order evolution equation for a thin, non-volatile, isothermal film, of viscosity μ, uniform surface tension σ and average depth ϵa (where $0 < \epsilon \ll 1$), lining the interior of a tube of uniform radius a. The tube has centreline curvature $\delta\kappa(s)/a$ where $0 < \delta \ll 1$ and $\kappa(s)$ is a non-dimensional $O(1)$ function of as, the arclength along the tube centreline. The tube centreline lies in a plane. The tube core contains a fluid (such as air) of viscosity $\gamma\mu$; provided $\gamma\epsilon \ll 1$ (Hammond 1983), the core fluid responds passively to any motion of the liquid lining, playing no role in the thin-film dynamics.

2.1. *Capillary statics*

For the curved interface of a thin film, the leading-order normal-stress condition reduces to a relation between fluid pressure and interfacial curvature. To compute this curvature, we introduce a curvilinear coordinate system, with non-dimensional independent variables (r, ϕ, s) (figure 1) with $0 \leqslant r \leqslant 1$, $0 \leqslant \phi < 2\pi$, $-\infty < s < \infty$, for which any small distance may be represented by

$$\mathrm{d}\boldsymbol{x} = a\left(\hat{\boldsymbol{r}}\,\mathrm{d}r + r\hat{\boldsymbol{\phi}}\,\mathrm{d}\phi + [1 + \delta\kappa(s) r \sin\phi]\,\hat{\boldsymbol{s}}\,\mathrm{d}s\right). \tag{2.1}$$

The unit normal to an interface $r = R(\phi, s)$ is then

$$\boldsymbol{n} = N\left\{\hat{\boldsymbol{r}} - \frac{R_\phi}{R}\hat{\boldsymbol{\phi}} - \frac{R_s}{\Delta}\hat{\boldsymbol{s}}\right\}, \qquad N \equiv \left[1 + \left(\frac{R_\phi}{R}\right)^2 + \left(\frac{R_s}{\Delta}\right)^2\right]^{-1/2}, \tag{2.2}$$

where $\Delta \equiv 1 + \delta\kappa(s) R \sin\phi$, and subscripts s and ϕ denote derivatives, so the interfacial curvature (scaled on a) is given by

$$a\nabla\cdot\boldsymbol{n} = \left(1 + \frac{\delta\kappa R \sin\phi}{\Delta}\right)\frac{N}{R} - \frac{1}{R\Delta}\left[\Delta N \frac{R_\phi}{R}\right]_\phi - \frac{1}{\Delta}\left(\frac{N}{\Delta}R_s\right)_s. \tag{2.3}$$

This reduces to the expression given by Hammond (1983), for example, if $\delta = 0$. Setting $R = 1 - \epsilon h(\phi, s)$, representing the interface of a film of thickness $\epsilon a h$, and taking terms up to leading order in ϵ and δ, the pressure in the fluid layer $(\sigma/a)p$ is given in non-dimensional terms by $p = -a\nabla\cdot\boldsymbol{n}$, i.e.

$$p = -\left[1 + \delta\kappa\sin\phi + \epsilon(h + h_{\phi\phi} + h_{ss})\right] \tag{2.4}$$

with error $O(\delta^2, \delta\epsilon, \epsilon^2)$, assuming that the pressure is zero in the core of the tube. This approximation is reliable provided ϵ/δ is neither too large nor too small, in which case higher-order effects of fluid thickness or curvature should be considered. The terms in (2.4) can be interpreted as follows: the -1 represents the dominant contribution to the subatmospheric fluid pressure coming from the almost uniform azimuthal curvature of the tube wall; the term of $O(\delta)$ shows that the pressure is

slightly lower (higher) on the outer (inner) wall of the tube, i.e. on O (I) in figure 1, because of centreline curvature; if the film thickens locally, its azimuthal radius of curvature falls and the pressure becomes more negative, an effect represented by the term ϵh, which is potentially destabilizing; interfacial curvature in the axial and azimuthal directions (represented by $h_{\phi\phi} + h_{ss}$) is stabilizing, however.

The effects of centreline curvature therefore appear as a body force, driving a flow from the inner to the outer wall (or, equivalently, from the outer to the inner wall if the fluid lines the exterior of the tube). There is a useful, mathematically analogous problem to consider at this stage. Suppose a straight, uniform cylindrical tube lies with its axis horizontal, lined on its interior with a thin layer of fluid that wets the wall; in the core of the tube is a gas of negligible density. Taking an azimuthal coordinate ϕ, with $\phi = -\frac{1}{2}\pi$ pointing upwards and $\phi = \frac{1}{2}\pi$ downwards in the direction of gravity g, the condition for hydrostatic equilibrium in the thin fluid layer of density ρ can be written to $O(\epsilon^2)$ as $p =$ constant where p is given by (2.4) with $\delta\kappa$ replaced by a Bond number $B = \rho a^2 g/\sigma$. Thus provided B and ϵ are of comparable magnitude, weak centreline curvature behaves just like a weak gravitational field, acting from the inner (upper) to the outer (lower) wall. Our results will therefore complement those of Reisfeld & Bankoff (1992), who examined gravity-driven flow of a thin film lining the exterior of a horizontal cylinder over a range of Bond numbers.

2.2. *Evolution equations*

Equation (2.4) can now be incorporated into the evolution equation for a thin fluid layer; for brevity we dispense with a formal derivation of the lubrication-theory approximation. (We shall obtain a particular limit of the evolution equation, recently derived by Roy, Roberts & Simpson (1996), for a thin film on a surface of arbitrary curvature.) The pressure in the fluid layer is uniform across the film at leading order. Inertia and gravity are neglected. The free surface of the fluid layer is taken to be free of tangential stress. The film is locally planar, so that the flow rate and mass conservation law for the fluid film are in non-dimensional terms (to leading order in ϵ)

$$h_t + \nabla_s \cdot \boldsymbol{q} = 0, \qquad \boldsymbol{q} = -\tfrac{1}{3} h^3 \nabla_s p, \tag{2.5}$$

where h now depends also on time t, which has been scaled on $\mu a/\sigma\epsilon^2$. The operator ∇_s represents the gradient along the surface of the curved tube, i.e. (from 2.1)

$$\nabla_s = \hat{\boldsymbol{\phi}} \frac{\partial}{\partial \phi} + \frac{\hat{\boldsymbol{s}}}{1 + \delta\kappa(s)\sin\phi} \frac{\partial}{\partial s}. \tag{2.6}$$

The volume flux $\boldsymbol{q}$ arises from flows driven by axial and azimuthal curvature (with velocities of dimensional magnitude $O(\epsilon^3\sigma/\mu)$) and from flows induced by centreline curvature (of comparable magnitude $O(\delta\epsilon^2\sigma/\mu)$).

The pressure gradient in (2.5) can be approximated to leading order using (2.4) and (2.6),

$$\nabla_s p = -\delta\hat{\nabla}(\kappa \sin\phi) - \epsilon\hat{\nabla}(h + \hat{\nabla}^2 h), \qquad \hat{\nabla} \equiv \hat{\boldsymbol{\phi}} \frac{\partial}{\partial \phi} + \hat{\boldsymbol{s}} \frac{\partial}{\partial s}, \tag{2.7}$$

so that (2.5) yields the leading-order evolution equation

$$h_t + \tfrac{1}{3}\delta\hat{\nabla} \cdot [h^3 \hat{\nabla}(\kappa \sin\phi)] + \tfrac{1}{3}\epsilon\hat{\nabla} \cdot \left[h^3 \hat{\nabla}(h + \hat{\nabla}^2 h)\right] = 0. \tag{2.8}$$

Setting $\delta = 0$ and neglecting any azimuthal dependence, we recover the evolution equation of Hammond (1983), Schwartz, Princen & Kiss (1986) and Yiantsios &

Higgins (1989)

$$h_t + \tfrac{1}{3}\epsilon \left[h^3 (h + h_{ss})_s\right]_s = 0, \tag{2.9}$$

which describes both the formation of thin, axisymmetric, wetting collars in straight tubes and the Rayleigh–Taylor instability of a thin fluid layer. The limit $\delta \to 0$ in (2.8) is singular, however, since even extremely weak centreline curvature breaks the symmetry of the problem and over sufficiently long times the solution structure is profoundly altered from the straight-tube case.

The presence of the $\sin\phi$ term in (2.8) is sufficient to drive an azimuthal draining flow, and if κ varies with s then an axial draining flow is also likely. The latter possibility was investigated by Schwartz & Weidner (1995) (see also Roy *et al.* 1996), who considered the evolution of a thin film on a solid surface with a single, non-uniform radius of curvature. However, henceforth we set $\kappa = 1$. In this case (2.8) is consistent with the evolution equation derived by Reisfeld & Bankoff (1992) for gravity-driven thin-film flow on a horizontal cylinder.

2.3. *Equilibrium solutions with zero contact angle*

In the thin-film limit there is no equilibrium h-distribution satisfying (2.8) in a uniformly curved tube for which the tube wall is everywhere wet. Reisfeld & Bankoff (1992) showed that steady, axially uniform solutions exist in the presence of stabilizing intermolecular forces or suitable thermocapillary effects, but neither effect is considered explicitly here. Instead we assume that the fluid wets the wall, i.e. that the fluid has zero contact angle at any static contact lines; numerical solutions of (2.8) in §3 below show that this is a natural and consistent boundary condition for solutions of this evolution equation. Then, if the tube is allowed to become dry over some portion of its wall, a variety of steady solutions of (2.8) can be found, particularly if we allow for axial variation. Assuming that δ and ϵ are both small, we seek (in §§4 and 5 below) constant-pressure solutions of (2.4) with wavelength L, applying zero contact angle at a static contact line $\phi = \alpha(s)$. Rescaling, setting $K = -(1+p)/\delta$, $H = (\epsilon/\delta)h$, (2.4) with $\kappa = 1$ becomes an inhomogeneous Helmholtz equation,

$$\sin\phi + H + H_{\phi\phi} + H_{ss} = K, \qquad \alpha(s) \leqslant \phi \leqslant \tfrac{1}{2}\pi, \qquad -\tfrac{1}{2}L \leqslant s \leqslant \tfrac{1}{2}L, \tag{2.10}$$

and solutions are sought subject to suitable no-flux and symmetry boundary conditions

$$H_s(\phi, -\tfrac{1}{2}L) = 0, \qquad H_s(\phi, \tfrac{1}{2}L) = 0, \qquad H_\phi(\tfrac{1}{2}\pi, s) = 0. \tag{2.11}$$

The zero-contact-angle condition is

$$H = 0, \qquad H_\phi - \alpha_s H_s = 0 \qquad \text{on} \qquad \phi = \alpha(s). \tag{2.12}$$

The fluid volume in one wavelength is represented by a parameter $\mathscr{V}$, where

$$\mathscr{V} \equiv \frac{V}{\pi\delta} = \frac{1}{\pi}\int_S H \,\mathrm{d}A \equiv \frac{2}{\pi}\int_{-L/2}^{L/2} \mathrm{d}s \int_{\alpha(s)}^{\pi/2} \mathrm{d}\phi \; H(\phi, s), \tag{2.13}$$

where S is the area of the wall per unit wavelength wetted by the fluid and $a^3 V$ the corresponding dimensional fluid volume. Integrating (2.10) over one wavelength and applying the divergence theorem, the pressure can be related to the fluid volume by

$$KS = \pi\mathscr{V} + \int_S \sin\phi \,\mathrm{d}A, \tag{2.14}$$

so that

$$K = \left(\tfrac{1}{2}\pi \mathscr{V} + \int_{-L/2}^{L/2} \cos\alpha(s)\, \mathrm{d}s \right) \Big/ \int_{-L/2}^{L/2} \left(\tfrac{1}{2}\pi - \alpha(s) \right) \mathrm{d}s. \tag{2.15}$$

Solutions of (2.10)–(2.15) are in general parameterized by L and $\mathscr{V}$; the unknowns are the film distribution H, the contact line location $\alpha(s)$ and the pressure variable K. These static solutions are all energy extrema; classical energetic arguments presented in Appendix A show that as $t \to \infty$, solutions of (2.8) evolve to a state of minimum energy, i.e. to one of the static solutions that exist for given L and $\mathscr{V}$.

2.4. *Axially uniform lobes*

The axially uniform equilibrium solution of (2.10)–(2.15) is

$$H_0(\phi) = K_0 - \tfrac{1}{2}(\tfrac{1}{2}\pi - \phi)\cos\phi + A_0 \sin\phi \tag{2.16}$$

for $\alpha_0 \leqslant \phi \leqslant \frac{1}{2}\pi$, where

$$A_0(\alpha_0) = -\tfrac{1}{2}\left\{1 + (\tfrac{1}{2}\pi - \alpha_0)\tan\alpha_0\right\}, \qquad K_0(\alpha_0) = \tfrac{1}{2}\left(\sin\alpha_0 + \frac{\frac{1}{2}\pi - \alpha_0}{\cos\alpha_0} \right). \tag{2.17}$$

Solutions for four values of α_0 are shown in figure 2(*a*). Assuming that a fluid layer of initially uniform thickness ($h = 1$, i.e. $H = \epsilon/\delta$, for which $\mathscr{V} = 2L\epsilon/\delta$) readjusts to form such a lobe (as demonstrated in §3 below), the volume of a uniform fluid lobe in a length L of tube is given by $\mathscr{V} = 2LV_0(\alpha_0)$, where (using 2.14)

$$V_0(\alpha_0) = \frac{1}{\pi}\int_{\alpha_0}^{\pi/2} H_0\, \mathrm{d}\phi = \frac{1}{\pi}\left[(\tfrac{1}{2}\pi - \alpha_0)K_0(\alpha_0) - \cos\alpha_0 \right], \tag{2.18}$$

so that the location of the contact line is defined by $V_0(\alpha_0) = \epsilon/\delta$. The function $V_0(\alpha_0)$ is monotonically decreasing as ϕ increases from $-\frac{1}{2}\pi$ to $\frac{1}{2}\pi$ (see figure 2*b*), so that for initially thicker (thinner) fluid layers or more weakly (strongly) curved tubes the contact line moves to the inner (outer) bend of the tube. For $\alpha_0 \to \frac{1}{2}\pi$, $V_0 \sim (\frac{1}{2}\pi - \alpha_0)^5/(45\pi)$, an approximation that works well for $\alpha_0 > 0$. The pressure variable K_0 is non-monotonic as α_0 increases (figure 2*c*), having a minimum value of $\frac{1}{4}\pi$.

In the singular limit $\delta \to 0$ the scalings used in (2.10) are inappropriate. Instead, letting $k = -(1 + p)/\epsilon$, the axially uniform solution $h = h_0(\phi)$, $k = k_0$, for which the contact-line conditions are $h_0 = h_{0\phi} = 0$ on $\phi = -\frac{1}{2}\pi$, is $h_0 = 1 + \sin\phi$, $k_0 = 1$, representing a cylindrical interface pinned to the line $\phi = -\frac{1}{2}\pi$.

3. Drainage in a curved tube

Suppose a semi-infinite bubble is blown slowly with steady speed U down a fluid-filled, weakly curved tube. At leading-order in capillary number (i.e. $Ca = \mu U/\sigma \ll 1$), the bubble nose forms a hemispherical cap that meets the tube wall with zero contact angle (Bretherton 1961). Because this interface meets the wall only along a circular effective contact line, the interface is unaffected (at this order) by the weak longitudinal curvature of the tube. A short transition region of length $O(Ca^{1/3})$ around the contact line, where the film has minimum thickness $O(Ca^{2/3})$, connects the 'capillary–statics' region around the bubble nose to a thin-film region upstream. Because the transition region is short, the dominant pressure gradient is an axial one associated with the

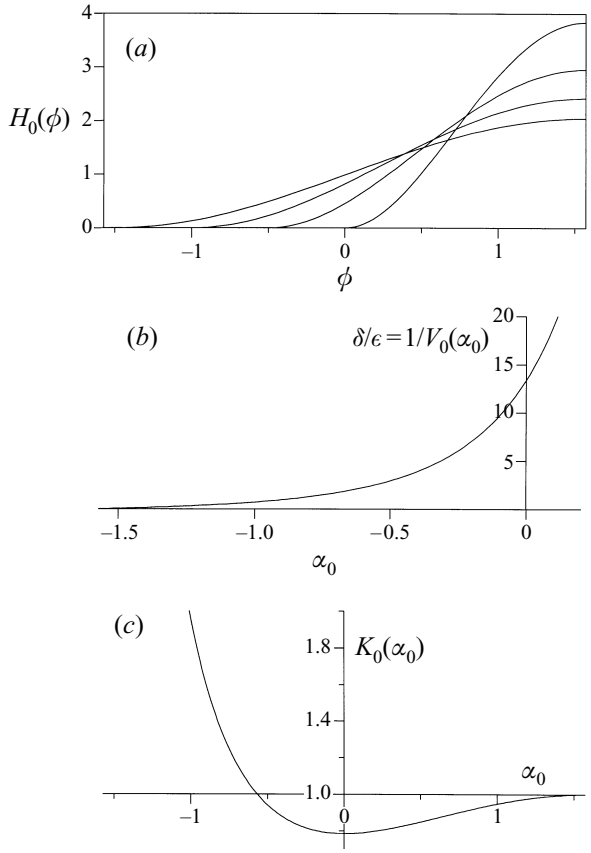

FIGURE 2. Equilibrium lobes: (*a*) equilibrium solutions for contact lines located at $\alpha_0 = -1.5$, -1, -0.5 and 0, for which $\delta/\epsilon = 0.0483$, 0.699, 2.938 and 13.44 respectively; (*b*) the relation between α_0 and δ/ϵ; (*c*) the pressure variable $K_0(\alpha_0)$.

curvature of the film in the axial direction; again, the effects of centreline curvature are not felt at leading order, so the fluid layer is azimuthally uniform to a good approximation. However, once the bubble has passed a given location, the effects of centreline curvature begin to be felt there, and the fluid layer slowly readjusts by draining from the inner to the outer wall of the tube. The key features of this draining flow are investigated below, under the assumption of axial uniformity. Solutions are presented for a surfactant-free (i.e. stress-free) air–liquid interface. Similar results should arise if a non-diffusing, insoluble surfactant is introduced at the free surface; since the draining flow is slow at large times, the surfactant distribution is likely to adjust relatively rapidly in response to the flow, assuming a quasi-steady, non-uniform distribution which effectively immobilizes the interface, reducing the fluid flux by up to a factor of four and increasing draining times accordingly. This possibility is not explored further here, however.

3.1. *Numerical solution*

The axially uniform, unsteady draining of a thin fluid layer from the inner to the outer wall of a uniformly curved tube is governed by

$$h_T + Q_\phi = 0, \qquad Q = -\tfrac{1}{3}h^3 P_\phi, \qquad P = -\left[C\sin\phi + h + h_{\phi\phi}\right], \tag{3.1}$$

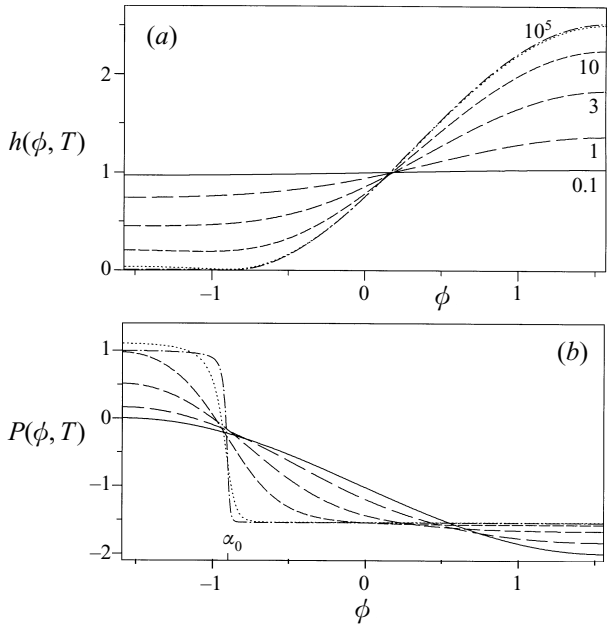

FIGURE 3. Draining flow for the case $C = 1$ at times $T = 0.1$, 1, 3, 10, 10^3 and 10^5: (*a*) film thickness h, (*b*) pressure P, plotted as functions of ϕ. The effective contact line is at $\alpha_0 = -0.881$.

where (2.4), (2.5) and (2.8) have been rescaled using $C \equiv \delta/\epsilon$, $Q = q/\epsilon$, $T = \epsilon t$ and $P = (1 + p)/\epsilon$. The fluid is assumed to wet the wall, and initially $h = 1$; no-flux boundary conditions are applied at $\phi = \pm\frac{1}{2}\pi$. Equations (3.1) were solved numerically in $-\frac{1}{2}\pi \leqslant \phi \leqslant \frac{1}{2}\pi$, using spatial finite differences and Gear's method in time. Similar computations, showing the early stages of the draining flow, have been presented by Reisfeld & Bankoff (1992) and Roy *et al.* (1996): here the interest is in the asymptotic behaviour at large times. Results for three representative cases, $C = 1$, $C = 2$ and $C = 10$, are shown in figures 3–5 respectively. In all cases (e.g. figure 3), fluid drains from the inner wall, leaving at large times a vanishingly thin layer in $-\frac{1}{2}\pi \leqslant \phi < \alpha_0$, accumulating as a near-equilibrium lobe on the outer wall (in $\alpha_0 < \phi \leqslant \frac{1}{2}\pi$) which corresponds to that computed in §2.4. However, the drainage takes infinite time, according to (3.1): the film thins significantly in the neighbourhood of $\phi = \alpha_0$, the resistance to flow rises dramatically there and the pressure drop between the fluid lobes on the inner and outer wall is concentrated in a narrowing region centred at $\phi = \alpha_0$ (figure 3*b*).

Reisfeld & Bankoff (1992) computed the location of the severest local film thinning as a function of the strength of the draining force (represented by C). Our computations confirm that the simple analytic relation $V_0(\alpha_0) = 1/C$ (see (2.18) and figure 2*b*) is sufficient to determine this relationship, at least in the absence of additional physical effects.

The rate of film thinning is plotted in figure 4, where the film thickness on the inner wall $h(-\frac{1}{2}\pi, T)$ and at the constriction $h_{min}(T)$ are plotted versus time on a logarithmic graph. The example chosen was for $C = 2$, which indicates how the thinning can have two distinct phases, the details of which are described below: once the film on the inner wall has thinned substantially, at intermediate times $h(-\frac{1}{2}\pi, T) \sim T^{-1/4}$ and $h_{min} \sim T^{-1/2}$, whereas at late times $h(-\frac{1}{2}\pi, T) \sim T^{-1/2}$ and $h_{min} \sim T^{-3/5}$. In figure 5

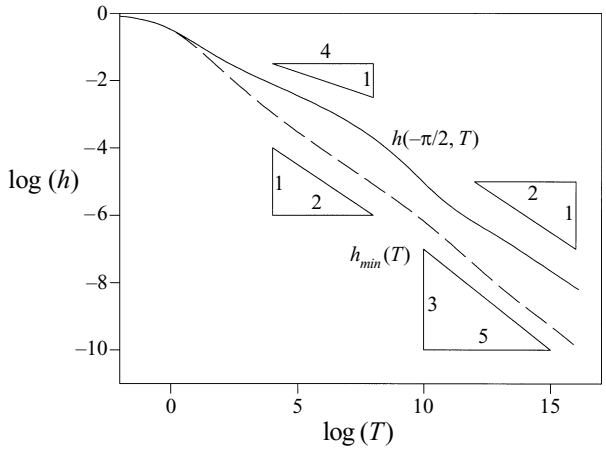

FIGURE 4. Thinning rates of draining flow for the case $C = 2$. The triangles indicate the slope of the intermediate- and late-time approximations.

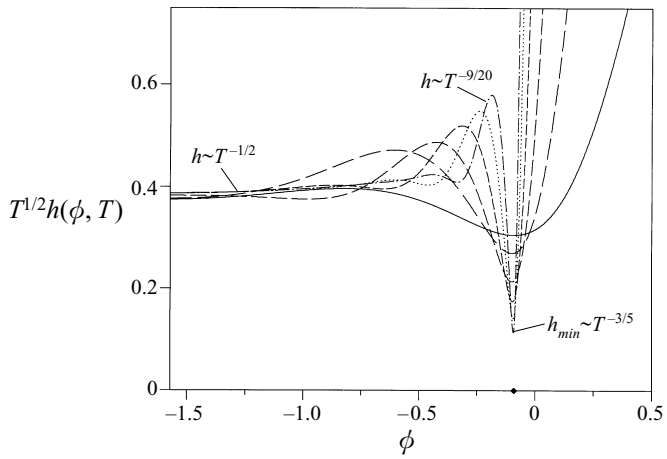

FIGURE 5. Draining of the inner-wall lobe in the case $C = 10$; $T^{1/2}h(\phi, T)$ is plotted versus ϕ for $T = 1$ (solid curve), 10, 10^2, 10^3, 10^4, 10^5 (dot-dash curve). The asymptotic scales of the dominant maximum and minimum are indicated. The effective contact line is at $\alpha_0 = -0.090$.

the film distribution on the inner wall, scaled by $T^{1/2}$, is plotted for $C = 10$; in this case the flow enters the late-time regime relatively quickly. A capillary wave develops upstream of the constriction, and the lengthscale of the waves shrinks as additional maxima and minima become more distinct. The detailed structure of this wave train is described below.

3.2. *Approximate solutions at large times*

There is a substantial body of work devoted to the asymptotic structure of draining flows, originating in studies by Frankel & Mysels (1962) and Princen (1963), and characteristic flow features (such as dimples) and scalings arise in many different contexts (e.g. foams, emulsions, the approach of a deformable bubble or drop towards a solid or fluid interface; see Yiantsios & Davis 1990 and references therein). Drawing on this work, a brief account of the approximate draining flows arising in the present draining problem is given here; some details are given in Appendix B.

Suppose that $C = O(1)$ or smaller. The primary difference between the two draining regimes shown in figure 4 is associated with the pressure (3.1) in the inner-wall draining region as $h \to 0$: in the intermediate-time draining regime, the contribution $-C\cos\phi$ to the pressure gradient P_ϕ (see 3.1) is weak, whereas in the late-time draining regime this term is dominant. The late-time approximation (§3.2.2 below) is a formal asymptotic solution of the problem: the transient intermediate-time solution (§3.2.1) is a formal asymptotic limit only for $C \ll 1$. However, since the intermediate-time scalings are exhibited even when $C = 2$ (figure 4), we can construct an *ad hoc* approximation (to be justified *a posteriori*) which contains as a special case the small-C limit.

3.2.1. *Intermediate-time approximation*

This approximation, which holds for $1 \ll T \ll T_{tr}(C)$, where the transition time T_{tr} is estimated below, resembles that described by Jones & Wilson (1978), Hammond (1983) and others. The fluid flux is everywhere $O(T^{-5/4})$, and the flow domain has three distinct regions.

(i) The emptying lobe on the inner wall in $-\frac{1}{2}\pi \leqslant \phi < \alpha_0$, in which the pressure is approximately uniform (as in figure 3*b*) and the film forms a spherical cap with $h \sim T^{-1/4}$ (figure 4), is given at leading order by

$$h = \frac{\beta}{T^{1/4}\cos\alpha_0}(\sin\alpha_0 - \sin\phi), \qquad P = -C\sin\phi - \frac{\beta}{T^{1/4}}\tan\alpha_0, \tag{3.2}$$

where $h_\phi(-\frac{1}{2}\pi) = 0$, $h(\alpha_0) = 0$ and $h_\phi(\alpha_0) = -\beta/T^{1/4}$, for some $\beta > 0$. The volume flux, given by $Q = -\int_{-\pi/2}^{\phi} h_T \,\mathrm{d}\phi$, is

$$Q = \frac{\beta}{4T^{5/4}}\left[(\tfrac{1}{2}\pi + \phi)\tan\alpha_0 + \frac{\cos\phi}{\cos\alpha_0}\right], \tag{3.3}$$

so the flux out of this region is $Q_0/T^{5/4}$ where $Q_0 = \frac{1}{4}\beta[1 + (\frac{1}{2}\pi + \alpha_0)\tan\alpha_0]$. Region (i) connects to

(ii) a short quasi-steady draining region, of length $O(T^{-1/4})$, in which $h \sim T^{-1/2}$ (figure 4) and there is an $O(1)$ pressure drop (figure 3*b*); setting

$$\phi = \alpha_0 + \frac{3Q_0}{\beta^4 T^{1/4}}\xi, \qquad h(\phi, t) = \frac{3Q_0}{\beta^3 T^{1/2}}\mathscr{H}(\xi), \qquad Q = \frac{Q_0}{T^{5/4}}, \tag{3.4}$$

to match with region (i), (3.1) reduces at leading order to

$$1 = \mathscr{H}^3\mathscr{H}_{\xi\xi\xi}, \quad \mathscr{H} \sim -\xi \text{ as } \xi \to -\infty, \quad \mathscr{H} \sim \tfrac{1}{2}\mathscr{C}\xi^2 \text{ as } \xi \to \infty, \quad \mathscr{H}_{min} = \mathscr{M}. \tag{3.5}$$

Equation (3.5) has a unique solution for which $\mathscr{C} \approx 1.2098$ and $\mathscr{M} \approx 1.2593$ (e.g. Wong, Radke & Morris 1995). This solution matches downstream onto

(iii) a quasi-static filling lobe on the outer wall of the tube in $\alpha_0 < \phi \leqslant \frac{1}{2}\pi$ in which $h \approx CH_0(\phi)$ (see (2.16) and figure 3). Matching the curvatures at α_0 (using (2.16)–(2.17)), the constant β is given by $K_0(\alpha_0) - \sin\alpha_0 = \mathscr{C}\beta^5/(3Q_0)$. The correction to the equilibrium solution is

$$h \sim CH_0(\phi) - \frac{4Q_0\sin\phi}{\cos\alpha_0\ T^{1/4}}. \tag{3.6}$$

To establish when this approximation fails, we can compare the flux (3.3) in (i) with an estimate of the flux, Q^U say, driven by the pressure gradient $-C\cos\phi$; Q^U

was neglected above. Putting the expression for h in (3.2) into $Q^U = \frac{1}{3}Ch^3\cos\phi$ yields

$$Q^U = \frac{C\beta^3}{3T^{3/4}}\frac{\cos\phi}{\cos^3\alpha_0}(\sin\alpha_0 - \sin\phi)^3. \tag{3.7}$$

The time T_{tr} can be estimated as that at which the fluxes (3.3) and (3.7), each averaged over region (i), are of equal magnitude. For $C \ll 1$, it can be shown that $T_{tr} \sim C^{-7}$; even for $C = 2$ (as in figure 4), $T_{tr} \approx 86$, indicating that the intermediate-time approximation retains its validity for a significant period in this case. Since $T_{tr} > 1$ for $C < 6.6$ (i.e. for $\alpha_0 < -0.22$), it is clear that for sufficiently large C the system passes directly into the late-time regime.

3.2.2. *Late-time approximation*

At sufficiently large times, the non-uniform pressure distribution in the inner-wall region drives a unsteady draining flow with flux $O(T^{-3/2})$. The solution is again analogous to the film drainage problem in droplet coalescence in the regime in which gravity drives a draining flow (Jones & Wilson 1978). This approximation is valid for $T \gg \max(T_{tr}, 1)$ if $C = O(1)$ and for $T \gg C^{-11}$ if $C \ll 1$.

(I) The unsteady emptying region on the inner wall in $-\frac{1}{2}\pi \leqslant \phi < \alpha_0$, in which $h \sim T^{-1/2}$ (as in figure 5), is governed (from (3.1)) at leading order by

$$h_T + \left[\tfrac{1}{3}Ch^3\cos\phi\right]_\phi = 0, \tag{3.8}$$

which has the similarity solution $h = S(\phi)/(CT)^{1/2}$ where $(S^3\cos\phi)_\phi = \frac{3}{2}S$, so that

$$S(\phi) = \frac{1}{(\cos\phi)^{1/3}}\left[\int_{-\pi/2}^{\phi}\frac{\mathrm{d}s}{(\cos s)^{1/3}}\right]^{1/2}. \tag{3.9}$$

For $\alpha_0 < 0$, this function is well approximated in $-\frac{1}{2}\pi \leqslant \phi < \alpha_0$ by

$$S(\phi) \sim \left(\tfrac{3}{2}\right)^{1/2} + \tfrac{1}{16}\left(\tfrac{3}{2}\right)^{1/2}(\phi + \tfrac{1}{2}\pi)^2 + \frac{43}{3584\sqrt{6}}(\phi + \tfrac{1}{2}\pi)^4 + O\left((\phi + \tfrac{1}{2}\pi)^6\right), \tag{3.10}$$

so that the fluid layer is of near-uniform thickness in this region. The flux out of the region is $\frac{1}{3}S_0^3\cos\alpha_0/(CT^3)^{1/2}$ where $S_0 = S(\alpha_0)$; fluid is driven into

(II) a short transition region near $\phi = \alpha_0$ of length $O(T^{-1/6})$ in which the pressure gradient due to curvature balances that due to azimuthal surface tension, generating a capillary wave train (figure 5). Setting

$$\phi = \alpha_0 + \frac{\xi}{(C^3T)^{1/6}}\left(\frac{S_0}{\cos\alpha_0}\right)^{1/3}, \qquad h(\phi, T) = \frac{S_0}{(CT)^{1/2}}G(\xi), \qquad Q = \frac{S_0^3\cos\alpha_0}{3(CT^3)^{1/2}}, \tag{3.11}$$

(3.1) becomes, at leading order,

$$1 = G^3(1 + G_{\xi\xi\xi}), \qquad G \to 1 \quad \text{as} \quad \xi \to -\infty, \qquad G \sim \tfrac{1}{2}\Lambda\xi^2 \quad \text{as} \quad \xi \to \infty, \tag{3.12}$$

where

$$\Lambda = (K_0 - \sin\alpha_0)\left[\frac{T}{S_0^2C^3\cos^4\alpha_0}\right]^{1/6}. \tag{3.13}$$

The downstream boundary condition, which matches onto the equilibrium region (III, below), is both weakly time-dependent (3.13) and a condition that does not strictly apply in the limit $\xi \to \infty$; this is a non-standard problem with a complicated structure (Wilson & Jones 1983), the details of which are given in Appendix B. There it is shown

that embedded in region (II) are a number of subregions (such as that representing the local maximum shown in figure 5 in which $h \sim T^{-9/20}$ over a lengthscale of $O(T^{-3/20})$), although the only region of practical interest is

(IIa) a quasi-steady drainage region, analogous to (ii) above, of length $O(T^{-3/10})$, in which $h \sim T^{-3/5}$ (see figures 4 and 5 and (B 4) below) over which there is an $O(1)$ pressure drop. This connects to

(III) a quasi-steady filling lobe on the outer wall of the tube in $\alpha_0 < \phi \leqslant \frac{1}{2}\pi$, in which $h \approx CH_0(\phi)$; the fluid volume approaches its equilibrium value like $T^{-1/2}$.

These asymptotics confirm that the lubrication-theory approximation remains self-consistent as the infinite-time singularity is approached, and that at large times it is reasonable to approximate the film distribution using the leading-order 'outer' solution, namely $h = 0$ in $-\frac{1}{2}\pi \leqslant \phi \leqslant \alpha_0$, $h = CH_0(\phi)$ in $\alpha_0 \leqslant \phi \leqslant \frac{1}{2}\pi$.

4. The stability of uniform lobes to axial perturbations

We now consider the stability of axially uniform equilibrium lobes, such as those shown in figure 2(*a*), which represent the asymptotic large-time solution resulting from the draining flow described in §3. A portion of the inner wall of the tube is treated as dry and the outer-wall lobe is assumed to wet the wall with zero contact angle. It is likely that provided δ is not too large, this lobe will be unstable to long-wavelength capillary disturbances. Since such lobes exist even in the limit $\delta \to 0$, we cannot recover directly the stability results of Goren (1962), say, for a cylindrical interface because (unlike Reisfeld & Bankoff 1992, who examined the stability of the near-uniform but unsteadily draining film) we are starting from a different basic state. The dynamic calculations of these authors apply to the initial evolution of the interface; here we are interested in any resulting equilibria, reached at a much later stage. We proceed by identifying the bifurcation structure of steady solution branches governed by (2.10)–(2.15), from which dynamic stability results can be inferred.

The linear stability of the uniform states is considered in §4.1 and weakly nonlinear theory is used to describe the branch of steady solutions near the critical wavenumber in §4.2; numerical finite-amplitude solutions are presented in §5 below.

4.1. *Linear stability theory*

We first perturb the uniform lobe, looking for marginally stable eigensolutions with period L. At a bifurcation point, two solutions co-exist for the same parameter values, so that the perturbation of the uniform state should have zero pressure and volume contribution at leading order. We set $H = H_0(\phi) + \varepsilon h_1(\phi)\cos(\lambda s)$ for some $\varepsilon \ll 1$, where $\lambda = 2\pi/L$, substitute this into (2.10)–(2.15) and linearize. The zero-pressure perturbation satisfies

$$(1-\lambda^2)h_1 + h_{1\phi\phi} = 0, \qquad h_{1\phi}(\tfrac{1}{2}\pi) = 0, \qquad \alpha_0 \leqslant \phi \leqslant \tfrac{1}{2}\pi, \tag{4.1}$$

so that

$$h_1 = A_1 \cos\left[(1-\lambda^2)^{1/2}(\tfrac{1}{2}\pi - \phi)\right] \tag{4.2}$$

for some constant A_1. The leading-order boundary condition at the contact line, $h_1(\alpha_0) = 0$ (a direct consequence of the zero-contact-angle condition), implies that

$$\lambda^2 = 1 - \left(1 - \frac{2\alpha_0}{\pi}\right)^{-2}. \tag{4.3}$$

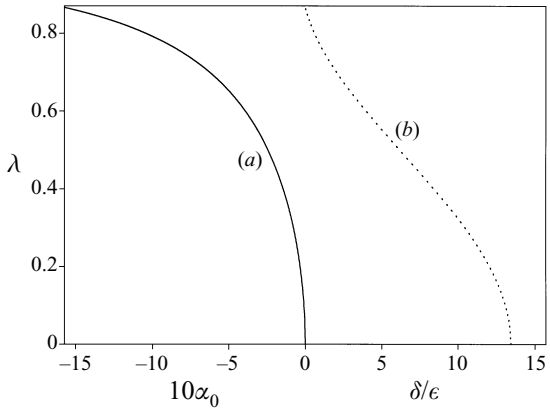

FIGURE 6. The critical wavenumber λ plotted against $10\alpha_0$ (a) and $C = \delta/\epsilon$ (b).

The critical wavenumber λ is plotted as a function of α_0 and of the corresponding value of δ/ϵ in figure 6. We anticipate that perturbations with wavenumbers in the range $(0, \lambda)$ will be unstable, with strictly positive growth rate. For very weak curvature ($\delta \to 0$), the lobe wets almost the entire tube wall ($\alpha_0 \to -\pi/2$) and $\lambda^2 \to \frac{3}{4}$; this differs from the classical result of Rayleigh (1879) for a straight cylindrical interface ($\lambda = 1$) because of the differing boundary condition at $\phi = -\frac{1}{2}\pi$, but is consistent with Davis (1980), who identified this as the critical wavenumber for a cylindrical rivulet pinned to a wire. Vanishingly small centreline curvature therefore reduces the range of unstable wavenumbers. As δ increases, more of the inner wall becomes dry and the range of unstable wavenumbers shrinks, until $\lambda = 0$ for $\alpha_0 = 0$; λ is not real for $\alpha_0 > 0$. Thus once some part of the outer wall becomes dry, the axially uniform lobe is linearly stable to capillary instability.

It is therefore possible to draw the neutral stability curve in $(L, \mathscr{V})$-parameter space, as shown by the curve NC_1 in figure 8 below. An axially uniform lobe with contact line at $\phi = \alpha_0$ is represented by the line $\mathscr{V} = 2LV_0(\alpha_0)$ in the $(L, \mathscr{V})$-plane, where V_0 is given by (2.18) (see also figure 2b). The neutral curve lies above the asymptotic boundaries of stability $\lambda^2 = \frac{3}{4}$ ($L = 4\pi/\sqrt{3}$) and $\alpha_0 = 0$ ($\mathscr{V} = L(\pi^2 - 8)/(4\pi)$), shown as dotted lines in figure 8. For fluid of fixed volume in a tube of fixed curvature, increasing the tube length L is both destabilizing (allowing capillary instabilities to develop) and also stabilizing (because the contact lines of the uniform lobe move from the inner to the outer wall of the tube). There is a minimum value of $\mathscr{V} \approx 3.718$ (at which $\alpha_0 \approx -0.1397$) below which the lobes are linearly stable. Neutral curves for solutions with wavelength $2L$ and $3L$ have also been plotted on figure 8 as curves NC_2 and NC_3 respectively, using the observation that any solution with parameters $(L, \mathscr{V})$ is equivalent to solutions with parameters $(nL, n\mathscr{V})$ for $n = 2, 3, \ldots$ etc.

We have not proved here that disturbances with wavelength longer than $2\pi/\lambda$ are unstable. However, using (2.8) one can compute the growth rate of linear perturbations to the static lobes (subject to suitable approximate conditions imposed at the contact line) and show that, as expected, positive growth rates exist for sufficiently long waves. This behaviour is entirely consistent with that expected from straight-tube calculations. The question of which wavelengths grow the fastest is not addressed in the present study, however, and the unsteady behaviour of the lining of a long curved tube remains to be investigated.

4.2. *Weakly nonlinear theory*

It is helpful before proceeding further to review the axisymmetric equilibrium fluid distributions that can arise in a straight cylindrical tube. Suppose a fluid of fixed volume a^3V lines the interior of a tube of length aL and radius a, with $V < \pi L$; L may be treated as a bifurcation parameter. For sufficiently small L the fluid lines the tube uniformly, with a cylindrical interface of radius $a\mathscr{R}$, say, where $0 < \mathscr{R} < L$. As L is increased through $2\pi\mathscr{R}$ this interface becomes unstable to axially varying perturbations. A branch of unduloids bifurcates from the cylindrical solutions at this critical wavelength. The wavelength of the unduloids falls as their amplitude grows from zero, making this bifurcation subcritical, and implying that the unduloids are unstable solutions. This is consistent with the work of Nayfeh (1970), who used the method of strained coordinates to demonstrate subcritical instability for an inviscid jet, and with Newhouse & Pozrikidis (1992), who showed numerically that a finite-amplitude unduloid solution is unstable in a related viscous problem. Provided $V < 1.74\pi$ (Everett & Haynes 1972), the unduloids can grow in amplitude until circular contact lines are formed around the tube, yielding localized collars (which, like the lobes in figure 2*a*, wet the tube wall with zero contact angle); these wetting-collar solutions are stable, representing the large-time asymptotic state reached after an axial draining flow similar to that described in §3 (Hammond 1983; Gauglitz & Radke 1988; Johnson *et al.* 1991). For $V \to 0$, which represents the thin-film limit studied by Hammond (1983), the unduloids and collars have constant wavelength 2π at leading order, so the bifurcation in this case is degenerate; higher-order terms in film thickness are required to show that it is subcritical.

By investigating (2.10)–(2.15) with the method of multiple scales, we seek to establish below whether the corresponding bifurcation of the axially uniform lobes in a curved tube are super- or subcritical, and hence whether the resulting wavy solutions are stable or unstable. Although supercritical behaviour might not be expected, it was demonstrated in a related problem by Brown & Scriven (1980), who studied wavy perturbations of an interface pinned to a slot.

We introduce two new variables, $x = s$ and $X = \varepsilon^2 s$, for some $\varepsilon \ll 1$. Hereafter, x and X are regarded as independent of each other, and solutions are sought with varying length. The uniform solution is perturbed as follows:

$$H(\phi, s) = H_0(\phi) + \varepsilon H_1(\phi, x, X) + \varepsilon^2 H_2(\phi, x, X) + \varepsilon^3 H_3(\phi, x, X) + O(\varepsilon^4), \tag{4.4}$$

$$\alpha(s) = \alpha_0 + \varepsilon\alpha_1(x, X) + \varepsilon^2\alpha_2(x, X) + \varepsilon^3\alpha_3(x, X) + O(\varepsilon^4), \tag{4.5}$$

$$K = K_0 + \varepsilon K_1 + \varepsilon^2 K_2 + \varepsilon^3 K_3 + O(\varepsilon^4), \tag{4.6}$$

with $-\frac{1}{2}\pi < \alpha_0 < 0$. At leading order we recover (2.16) and (2.17), noting that $H_0'' \equiv H_{0\phi\phi}(\alpha_0) > 0$ and $H_0''' \equiv H_{0\phi\phi\phi}(\alpha_0) < 0$. It is convenient in the remainder of this section to parameterize solutions by α_0, rather than the volume $\mathscr{V}$: in this way, increasing L is always destabilizing. We therefore impose the constraint $\mathscr{V} = 2LV_0(\alpha_0)$, which is equivalent to crossing the neutral curve in figure 8 along a straight line passing through the origin of the $(L, \mathscr{V})$-plane.

At $O(\varepsilon)$, (2.10) gives

$$H_1 + H_{1xx} + H_{1\phi\phi} = K_1, \qquad H_{1\phi}(\tfrac{1}{2}\pi, x, X) = 0 \tag{4.7}$$

with

$$H_1(\alpha_0, x, X) = 0, \qquad \alpha_1 H_0'' + H_{1\phi}(\alpha_0, x, X) = 0, \tag{4.8}$$

which has the separable solution (as in §4.1)

$$H_1(\phi, x, X) = \mathscr{A}(X)\cos\left[(1-\lambda^2)^{1/2}(\tfrac{1}{2}\pi - \phi)\right]\cos\left[\lambda x + \Theta(X)\right], \qquad K_1 = 0 \tag{4.9}$$

for some amplitude and phase functions $\mathscr{A}$ and Θ, where $\lambda(\alpha_0)$ satisfies (4.3) and

$$\alpha_1(x, X) = \frac{-\mathscr{A}(X)(1-\lambda^2)^{1/2}\cos\left[\lambda x + \Theta(X)\right]}{H_0''}. \tag{4.10}$$

Thus $H_{1x} = 0$ and $H_{1\phi\phi} = 0$ along $\phi = \alpha_0$, while $H_{1\phi} = -\alpha_1 H_{0\phi\phi}$ there.

At $O(\varepsilon^2)$ we have

$$H_2 + H_{2xx} + H_{2\phi\phi} = K_2, \qquad H_{2\phi}(\tfrac{1}{2}\pi, x, X) = 0, \tag{4.11}$$

and along $\phi = \alpha_0$

$$\tfrac{1}{2}\alpha_1^2 H_0'' + \alpha_1 H_{1\phi} + H_2 = 0, \qquad \alpha_2 H_0'' + \tfrac{1}{2}\alpha_1^2 H_0''' + H_{2\phi} = 0. \tag{4.12}$$

The first boundary condition in (4.12) becomes $H_2 = \frac{1}{2}\alpha_1^2 H_0''$, i.e.

$$H_2(\alpha_0, x, X) = B^2\cos^2(\lambda x + \Theta), \qquad B^2 = \mathscr{A}^2(1-\lambda^2)/(2H_0''), \tag{4.13}$$

so that H_2 is forced by terms of the form 1 and $\cos(2\lambda x + 2\Theta)$, yielding regular solutions of (4.11). Defining

$$F(\phi;\lambda) = \begin{cases} \cos\left[(1-\lambda^2)^{1/2}(\tfrac{1}{2}\pi - \phi)\right] & \text{for } 0 < \lambda \leqslant 1 \\ \cosh\left[(\lambda^2-1)^{1/2}(\tfrac{1}{2}\pi - \phi)\right] & \text{for } \lambda > 1, \end{cases} \tag{4.14}$$

the solution of (4.11)–(4.13) can be written

$$H_2(\phi, x, X) = K_2 + (\tfrac{1}{2}B^2 - K_2)\frac{\sin\phi}{\sin\alpha_0} + \tfrac{1}{2}B^2\frac{F(\phi, 2\lambda)}{F(\alpha_0, 2\lambda)}\cos\left[2\lambda x + 2\Theta\right]. \tag{4.15}$$

The remaining boundary condition in (4.12) gives

$$\alpha_2(x, X) = -\frac{B^2}{2H_0''}\left[\frac{H_0'''}{H_0''} + \frac{1-(2K_2/B^2)}{\tan\alpha_0} - \mathscr{T}\cos\left[2\lambda x + 2\Theta\right]\right] \tag{4.16}$$

where

$$\mathscr{T} = -\frac{H_0'''}{H_0''} + \begin{cases} (4\lambda^2-1)^{1/2}\tanh\left[(4\lambda^2-1)^{1/2}(\tfrac{1}{2}\pi - \alpha_0)\right] & \text{for } \tfrac{1}{4} < \lambda^2 < \tfrac{3}{4} \\ -(1-4\lambda^2)^{1/2}\tan\left[(1-4\lambda^2)^{1/2}(\tfrac{1}{2}\pi - \alpha_0)\right] & \text{for } 0 < \lambda^2 \leqslant \tfrac{1}{4}. \end{cases} \tag{4.17}$$

To complete the second-order solution, K_2 in (4.15) and (4.16) is determined by the volume constraint $\mathscr{V} = 2LV_0(\alpha_0)$. Expanding the integral for $\mathscr{V}$ using (4.4) and (4.5) in (2.13), retaining terms up to $O(\epsilon^2)$, the constraint yields the condition

$$\int_{-\pi/\lambda}^{\pi/\lambda}\left[\tfrac{1}{2}V_0''(\alpha_0)\alpha_1^2 + V_0'(\alpha_0)\alpha_2\right]\,\mathrm{d}s + \frac{1}{\pi}\int_{-\pi/\lambda}^{\pi/\lambda}\mathrm{d}s\int_{\alpha_0}^{\pi/2}\mathrm{d}\phi\; H_2 = 0 \tag{4.18}$$

from which $K_2(\alpha_0)$ is found to be

$$K_2 = \frac{B^2}{2}\frac{\left[1-(\pi V_0'/H_0'') + (\pi\tan\alpha_0/H_0''^2)\left(V_0''H_0'' - V_0'H_0'''\right)\right]}{\left[1-(\pi V_0'/H_0'') - \tan\alpha_0\left(\tfrac{1}{2}\pi - \alpha_0\right)\right]}. \tag{4.19}$$

At third order,

$$H_3 + H_{3xx} + H_{3\phi\phi} + 2H_{1xX} = K_3, \qquad H_{3\phi}(\tfrac{1}{2}\pi, x, X) = 0, \tag{4.20}$$

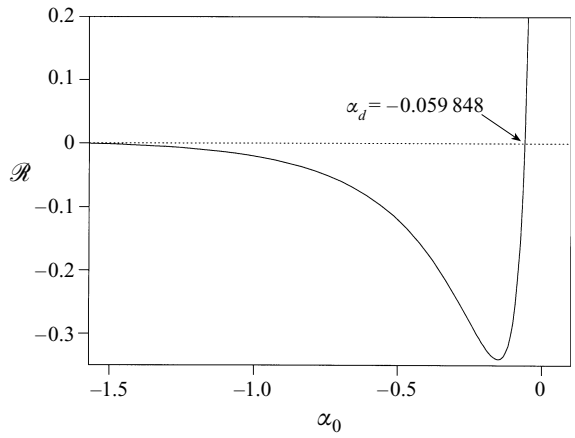

FIGURE 7. The function $\mathscr{R}(\alpha_0)$.

and along $\phi = \alpha_0$ only one boundary condition need be considered,

$$H_3 + \alpha_1 H_{2\phi} + \alpha_2 H_{1\phi} + \alpha_1\alpha_2 H_0'' + \tfrac{1}{6}\alpha_1^3 H_0''' = 0, \tag{4.21}$$

which may be simplified to $H_3(\alpha_0, x, X) = \alpha_1\alpha_2 H_0'' + \frac{1}{3}\alpha_1^3 H_0'''$. Thus from (4.10) and (4.16), H_3 is forced by terms of the form $\mathscr{A}^3\cos(\lambda x + \Theta)$ and $\mathscr{A}^3\cos(3\lambda x + 3\Theta)$. The secular forcing terms must be suppressed by a suitable choice of $\mathscr{A}$ and Θ. Since H_{1xX} has two terms, one involving $\mathscr{A}_X\sin(\lambda x + \Theta)$ and the other $\Theta_X\cos(\lambda x + \Theta)$, we set $\mathscr{A}_X = 0$ and then balance the terms in $\cos(\lambda x + \Theta)$.

The secular boundary-condition terms in (4.21) are of the form $\mathscr{R}\mathscr{A}^3\cos(\lambda x + \Theta)$ where

$$\mathscr{R} = \frac{(1-\lambda^2)^{3/2}}{4H_0''^2}\left[\frac{\frac{1}{2}\pi - \alpha_0 + (\pi/H_0''^2)(V_0''H_0'' - V_0'H_0''')}{(\frac{1}{2}\pi - \alpha_0)\tan\alpha_0 - 1 + (\pi V_0'/H_0'')} - \frac{\mathscr{T}}{2}\right] \tag{4.22}$$

with $\mathscr{T}$ given by (4.17). Figure 7 shows that $\mathscr{R} < 0$ for $-\frac{1}{2}\pi < \alpha_0 < \alpha_d$, and $\mathscr{R} > 0$ for $\alpha_d < \alpha_0 < 0$ where $\alpha_d \approx -0.059848$. The corresponding contribution to H_3 is of the form $\mathscr{F}(\phi)\cos(\lambda x + \Theta)$, where

$$(1-\lambda^2)\mathscr{F} + \mathscr{F}_{\phi\phi} = 2\lambda\Theta_X\mathscr{A}\cos\left[(1-\lambda^2)^{1/2}(\tfrac{1}{2}\pi - \phi)\right] \tag{4.23}$$

where $\mathscr{F}_\phi(\frac{1}{2}\pi) = 0$ and $\mathscr{F}(\alpha_0) = \mathscr{R}\mathscr{A}^3$. The appropriate solution is

$$\mathscr{F} = -\lambda\mathscr{A}\Theta_X(1-\lambda^2)^{-1/2}(\phi - \tfrac{1}{2}\pi)\sin\left[(1-\lambda^2)^{1/2}(\tfrac{1}{2}\pi - \phi)\right], \tag{4.24}$$

so the remaining boundary condition implies that

$$\mathscr{R}\mathscr{A}^2 = \lambda\Theta_X(1-\lambda^2)^{-1/2}(\tfrac{1}{2}\pi - \alpha_0). \tag{4.25}$$

Since $\mathscr{A}$ is independent of X, we can integrate (4.25), imposing $\Theta = 0$ at $X = 0$, so that the slowly varying phase is given by

$$\Theta(X) = \frac{\mathscr{R}\mathscr{A}^2(1-\lambda^2)^{1/2}}{\lambda(\frac{1}{2}\pi - \alpha_0)}X. \tag{4.26}$$

Then in the leading-order expression for the film depth,

$$H = H_0(\phi) + \varepsilon\mathscr{A}\cos\left[(1-\lambda^2)^{1/2}(\tfrac{1}{2}\pi - \phi)\right]\cos\left[\lambda s\left(1 + \frac{\varepsilon^2\mathscr{R}\mathscr{A}^2(1-\lambda^2)^{1/2}}{\lambda^2(\frac{1}{2}\pi - \alpha_0)}\right)\right] + O(\varepsilon^2), \tag{4.27}$$

the wavelength of the unduloid is related to the amplitude $\varepsilon\mathscr{A}$ by

$$L = \frac{2\pi}{\lambda}\left(1 - \frac{(\varepsilon\mathscr{A})^2\mathscr{R}(1-\lambda^2)^{1/2}}{\lambda^2(\frac{1}{2}\pi - \alpha_0)}\right). \tag{4.28}$$

Thus where $\mathscr{R} < 0$ (figure 7), the wavy lobe lengthens as it grows in amplitude along a line $\mathscr{V} = 2LV_0(\alpha_0)$; treating the wavelength as a bifurcation parameter, this is therefore a supercritical bifurcation at the critical point, and the branch of steady unduloids is stable to small perturbations. Where $\mathscr{R} > 0$, the bifurcation is subcritical and the branch of wavy solutions is unstable. The transition between the two types of behaviour is indicated with a bullet on the curve NC_1 (and similarly on NC_2) in figure 8: it occurs at $\mathscr{V} \approx 4.246$, $L \approx 23.41$. As $\alpha_0 \to -\frac{1}{2}\pi$, representing the limit of zero centerline curvature, $\mathscr{R} \to 0$, so the bifurcation is degenerate in this singular limit.

5. Finite-amplitude equilibria

5.1. *Wavy lobes*

We seek finite-amplitude solutions of the nonlinear free-boundary problem defined by (2.10)–(2.15). The separable solution of (2.10) and (2.11) in Cartesian coordinates is

$$H = K - \tfrac{1}{2}(\tfrac{1}{2}\pi - \phi)\cos\phi + A\sin\phi + \sum_{n=1}^{\infty} A_n F(\phi;\lambda_n)\cos\lambda_n s, \qquad \lambda_n = \frac{2n\pi}{L}, \tag{5.1}$$

for $\alpha(s) \leqslant \phi \leqslant \frac{1}{2}\pi$ and $-\frac{1}{2}L \leqslant s \leqslant \frac{1}{2}L$, where F is given by (4.14) and K by (2.15). The first three terms contribute to (2.16); the $n = 1$ term corresponds to the marginally stable mode from linear stability theory (4.2). To impose the contact-line boundary conditions (2.12) a numerical procedure is necessary. We follow Tuck & Schwartz (1991) and discretize the boundary with N grid points at axial locations between $s = 0$ and $s = \frac{1}{2}L$ (exploiting symmetry as far as possible), so that N unknowns describe the location of the interface. Truncating the series in (5.1) at $n = N - 1$ (giving N unknowns A, $A_1, \ldots, A_{N-1}$) yields $2N$ unknowns in all. The two boundary conditions (2.12) applied at each node on the boundary provide $2N$ nonlinear algebraic equations for these unknowns, which can be solved with Newton's method. The NAG routine C05PCF was employed, and the Jacobian for the problem was determined explicitly.

The fluid volume $\mathscr{V}$ and the domain length L were fixed at the start of a calculation. The wavy solution branch near the neutral curve was found using the eigensolution from linear stability analysis in §4.1, and path-tracking methods were used to follow the solution to large amplitudes. Typically 20 grid points (plus 20 coefficients in (5.1)) gave reliable results: accuracy was ensured where possible using grid refinement. However, the numerical method was prone to an instability in certain regimes of parameter space (in particular, the points marked with small circles along curve D in figure 8, see §5.3 below), manifesting itself as grid-scale wiggles, possibly arising from ill-conditioning. For fixed L and $\mathscr{V}$ the instability became progressively worse as N

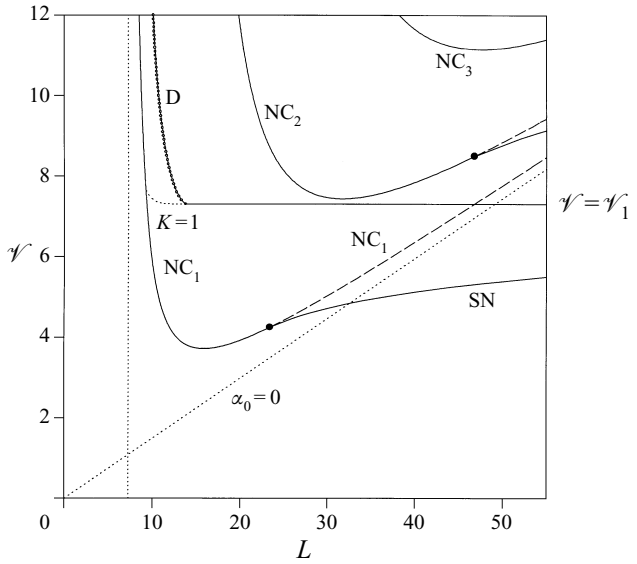

FIGURE 8. Stability boundaries in $(L, \mathscr{V})$-parameter space. Beneath the neutral curve NC_1 axially uniform lobes are linearly stable; wavy solutions bifurcate supercritically (subcritically) where NC_1 is solid (dashed); the saddle-node curve SN emerges from the codimension-2 point (marked with a bullet). The asymptotes of NC_1 are shown as dotted lines. Stable wavy solutions exist in the region bounded by NC_1 where it is solid, the fold curve SN, the drop boundary D and the line $\mathscr{V} = \mathscr{V}_1$. Both SN and the line $K = 1$ (shown dotted) asymptote to $\mathscr{V} = \mathscr{V}_1$ as $L \to \infty$. Localized drops exist to the right of D for $\mathscr{V} > \mathscr{V}_1$. Wavy solutions with wavelength nL exist above NC_n for $n = 2, 3$.

was increased. It could be suppressed to a certain extent by using a non-uniform grid with only a modest loss of accuracy, and by this means it was possible to identify the key features of parameter space satisfactorily.

Wavy solutions were found to bifurcate super- or subcritically along the neutral curve NC_1 in figure 8, as predicted by the analysis of §4. Bifurcation diagrams for the case $\mathscr{V} = 5$ are shown in figure 9, where K and the amplitude of contact-line variation $\Delta\alpha = |\alpha(\frac{1}{2}L) - \alpha(0)|$ are plotted versus L: as the tube length is increased, the initially uniform lobe first loses stability (at $L \approx 10.72$) to a branch of stable, wavy solutions through a supercritical pitchfork bifurcation; this wavy branch terminates at a saddle-node bifurcation at $L \approx 36.47$, where it meets an unstable branch of wavy solutions which bifurcates subcritically from the uniform-lobe branch at $L \approx 29.80$. The saddle-node point was tracked numerically across parameter space and is shown as the curve SN on figure 8, emanating from the codimension-2 point on the neutral curve. For large L there is hysteresis in the transitions between uniform and wavy states (figure 9), and for points lying between the curves NC_1 and SN in figure 8 there exist three steady states, two of which are linearly stable. Figure 9(*a*) shows how the pressure of the uniform solution is non-monotonic as L increases and the contact line moves from the inner to the outer wall (see figure 2*c*): K falls to its minimum value $\frac{1}{4}\pi$ at $L \approx 33.61$.

Examples of wavy lobe solutions along the line $\mathscr{V} = 5$ are shown in figure 10(*a–c*). A small-amplitude solution ($L = 10.8$, figure 10*a*) shows a weak bulge in the contact line where the film is thickest. Further along the wavy solution branch ($L = 15$, figure 10*b*), the distortion of the lobe is much more pronounced, and the film has become very thin at each end of the domain ($H(\frac{1}{2}\pi, \frac{1}{2}L) \approx 0.0502$). As L

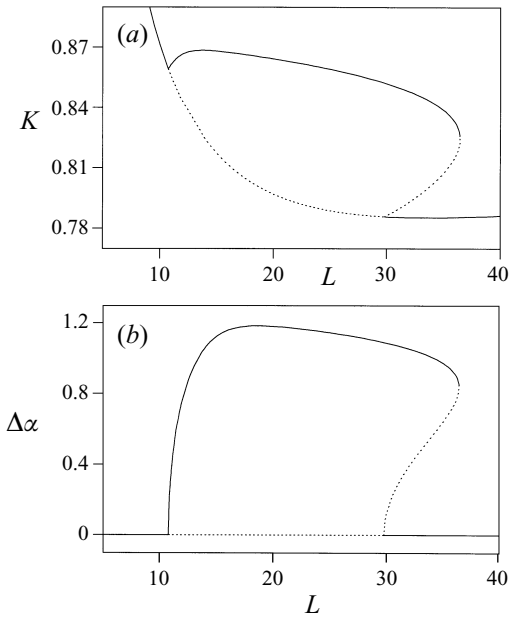

FIGURE 9. Bifurcation diagrams for the case $\mathscr{V} = 5$: solid curves show stable solution branches, dashed curves represent unstable solutions: (*a*) the pressure variable K and (*b*) and contact line amplitude $\Delta\alpha = |\alpha(0) - \alpha(\frac{1}{2}L)|$ are plotted against L.

increases further (e.g. $L = 30$, figure 10*c*), the amplitude and pressure of the solution change very little (figure 9), but the solution develops a solitary structure, with long, thin arms that extend to either side of the blob of fluid centred on $s = 0$; in this case $H(\frac{1}{2}\pi, \frac{1}{2}L) = 0.0550$. The arms correspond closely to the uniform-lobe solution (2.16), (2.17) having the same pressure as the wavy solution, i.e. $K \approx K_0(\alpha_c)$, where $\alpha_c = \alpha(\frac{1}{2}L)$.

5.2. *Solitary solutions*

The behaviour of solitary solutions such as that in figure 10(*c*) can be understood by fixing L and varying $\mathscr{V}$. Bifurcation diagrams for the case $L = 30$ are shown in figure 11. At small $\mathscr{V}$ the fluid is confined to a uniform lobe that lies entirely on the outer wall of the tube. As $\mathscr{V}$ increases through 4.463 the contact line of this lobe moves onto the inner wall, and the pressure in the lobe falls (i.e. K in figure 11*a* rises). Shortly afterwards, at $\mathscr{V} \approx 5.026$, the uniform lobe loses stability to an unstable branch of wavy lobes, which corresponds to crossing NC_1 in figure 8. This unstable branch and a large-amplitude stable wavy-solution branch (see $\Delta\alpha$ in figure 11*b*) originate at a saddle-node bifurcation at $\mathscr{V} \approx 4.713$. Along the stable branch, solutions have a solitary structure such as that shown in figure 10(*c*) for $\mathscr{V} = 5$. As $\mathscr{V}$ increases, K increases towards 1 (figure 11*a*) and the arm half-width $\hat{\alpha} = \frac{1}{2}\pi - \alpha_c$ shrinks to zero (figure 11*c*). From (2.16)–(2.18), one can show that in the limit $\hat{\alpha} \to 0$, the arms have the asymptotic structure

$$H_0(\phi) \sim \tfrac{1}{24}\left[\hat{\alpha}^2 - (\tfrac{1}{2}\pi - \phi)^2\right]^2, \qquad K_0(\alpha_c) \sim 1 - \tfrac{1}{6}\hat{\alpha}^2, \qquad V_0(\alpha_c) \sim \frac{\hat{\alpha}^5}{45\pi}, \tag{5.2}$$

where $|\frac{1}{2}\pi - \phi| \leqslant \hat{\alpha}$. Thus the film height, of $O(\hat{\alpha}^4)$, falls to zero much faster than the arm-width $2\hat{\alpha}$ shrinks, and the volume of fluid in the arms falls very rapidly. A typical

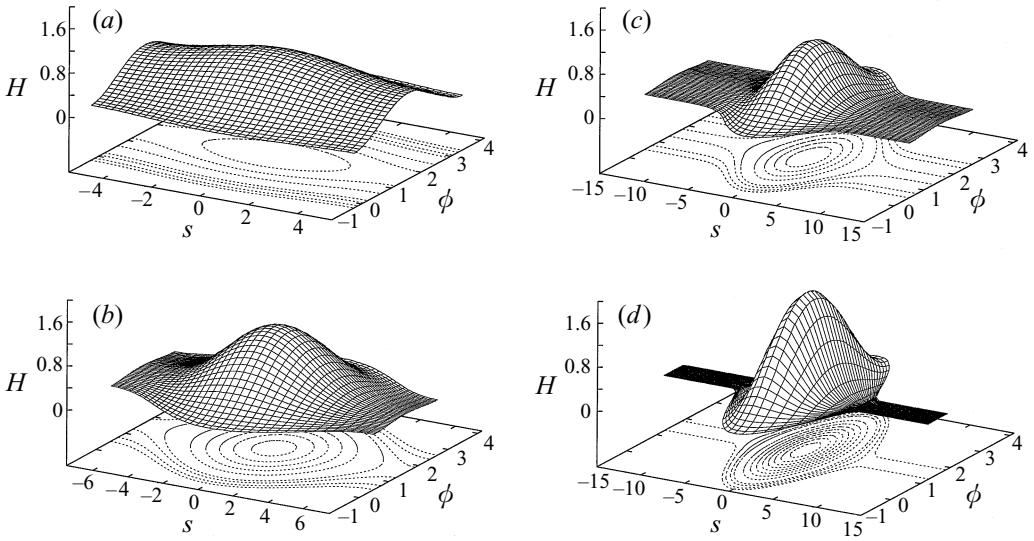

FIGURE 10. Wavy lobe solutions for $\mathscr{V} = 5$ with $N = 20$, showing film depth H against ϕ and s for (*a*) $L = 10.8$, (*b*) $L = 15$, (*c*) $L = 30$. Panel (*d*) shows a solution with $L = 30$, $\mathscr{V} = 7$ and $N = 20$. Different s-scales are used in each figure; contours are plotted beneath each surface at $H = 0$, 0.01, 0.05, 0.1, 0.3, 0.5, ... where appropriate.

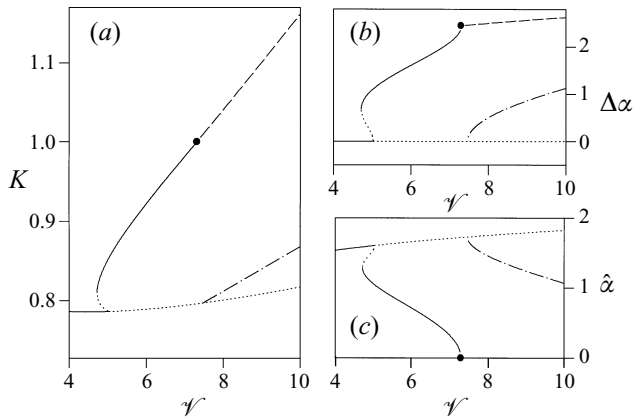

FIGURE 11. Bifurcation diagrams for the case $L = 30$: solid curves show stable uniform or wavy solution branches; dotted curves represent unstable solutions; dashed curves represent stable localized drop solutions; the dot-dash curves represent the wavy solution branch with wavelength $L = 15$. Panels show (*a*) the pressure variable K, (*b*) the contact-line amplitude $\Delta\alpha = |\alpha(\frac{1}{2}L) - \alpha(0)|$ and (*c*) the arm half-width $\hat{\alpha} = \frac{1}{2}\pi - \alpha_c$, all plotted against $\mathscr{V}$. Bullets mark the point at which the solution changes topology, becoming a localized droplet.

solution is shown in figure 10(*d*), for which $\mathscr{V} = 7$: in this case, $H(\frac{1}{2}\pi, \frac{1}{2}L) \approx 0.00049$. Because the film becomes so thin, the numerical method breaks down before $K \to 1$: extrapolation of the results in figure 11 suggest that this limit is reached as $\mathscr{V} \to 7.30$. The behaviour of the fluid blob for larger $\mathscr{V}$, once the arms have vanished (represented by the dashed line in figure 11), is discussed in §5.3 below. Also shown in figure 11 with a dot-dashed line is the branch of wavy lobes with wavelength $L = 15$, which

bifurcates supercritically from the axially uniform solution on crossing the curve NC_2 (see figure 8).

The asymptotic behaviour of the solitary solutions (e.g. figure 10*c*, *d*) can be exploited to infer some important features of the stability diagram in figure 8. Consider the branch of wavy solutions along a line $L = L_b$, say (e.g. $L = 30$, figure 11), parameterized by varying volume. Suppose that for $\mathscr{V} = \mathscr{V}_b$, say, the wavy solution has a solitary structure and pressure $K = K_b$ where $\frac{1}{4}\pi < K_b < 1$, so that $K_b = K_0(\alpha_c)$ (see (2.17) and figure 2*c*). These arms can be extended indefinitely beyond $s = \pm\frac{1}{2}L$ without the pressure or the amplitude of the solution changing. Since the arms occupy volume $2V_0(\alpha_c)$ per unit length (see (2.18)), there exists a family of solutions for $L > L_b$ with constant amplitude and pressure along the line in $(\mathscr{V}, L)$-parameter space given by

$$\mathscr{V} = \mathscr{V}_b + 2V_0(\alpha_c)\,(L - L_b)\,. \tag{5.3}$$

By computing a sequence of solitary solutions along the line $L = L_b$, and hence a set of lines (5.3), we can construct much of the surface of wavy solutions for larger L. It is possible, for example, to find where neighbouring lines of constant pressure and amplitude given by (5.3) intersect; the envelope of such intersections corresponds to the curve SN in figure 8, which marks a fold in the solution surface. Treating $\mathscr{V}_b$ as a function of α_c alone, this curve is defined parametrically by

$$L = L_b - \frac{\mathscr{V}_b'(\alpha_c)}{2V_0'(\alpha_c)}, \qquad \mathscr{V} = \mathscr{V}_b - V_0(\alpha_c)\frac{\mathscr{V}_b'(\alpha_c)}{V_0'(\alpha_c)}. \tag{5.4}$$

Note that $V_0'(\alpha_c) < 0$ (figure 2*b*), and $\mathscr{V}_b'(\alpha_c) > 0$. Explicit computations of the location of the fold-curve SN agree very well with this asymptotic approach using $L_b = 34$.

As $\alpha_c \to \frac{1}{2}\pi$, the slope $2V_0(\alpha_c)$ of a constant-amplitude line (5.3) in $(L, \mathscr{V})$-space tends rapidly to zero (see (5.2)). In the limit, therefore, there is a line in parameter space, $\mathscr{V} = \mathscr{V}_1$, say, for $L > L_b$, along which $K = 1$ and for which the solitary solutions have vanishingly narrow arms. From figure 11, $\mathscr{V}_1 \approx 7.30$. Using (5.4), it can be shown that the curve SN given by (5.4) asymptotes to the line $\mathscr{V} = \mathscr{V}_1$ as $L \to \infty$ (see figure 8). The location of the line $K = 1$ for smaller values of L was determined by computing appropriate wavy solutions with $9.256 \leqslant L \leqslant 13.75$, and is shown by a short dotted line in figure 8. It asymptotes rapidly to the boundary $\mathscr{V} = \mathscr{V}_1$ as L increases, implying that the asymptotic solitary solution structure exists for a wide range of L. It is shown below that the boundary $\mathscr{V} = \mathscr{V}_1$ represents an important change in the liquid-lining topology, separating wavy solitary solutions from localized droplets.

5.3. *Localized droplets*

In a straight tube, a sufficiently small volume of fluid can form a single localized, axisymmetric, stable wetting collar (Everett & Haynes 1972; Hammond 1983) which has two circular contact lines and which wets the wall between them; the wall is effectively dry beyond. If the tube has radius a and length aL, the contact lines are a distance $2\pi a$ apart and the collar can be regarded as an equilibrium fluid distribution for all $L \geqslant 2\pi$. Such localized solutions can exist because the azimuthal curvature term ϵh in (2.4), which tends to draw the interface towards the centre of the tube, competing against the axial curvature term ϵh_{ss}, has the capacity to confine a small volume of fluid to a finite length of tube. If a collar is perturbed very weakly, either by centreline curvature or gravity, a draining flow from the inner to the outer wall

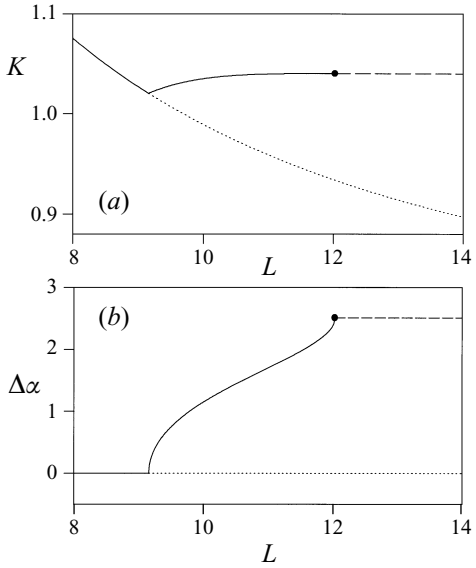

FIGURE 12. Bifurcation diagram for $\mathscr{V} = 8$, computed with $N = 16$, showing (*a*) pressure K and (*b*) amplitude $\Delta\alpha$: solid (dotted) lines show stable (unstable) uniform or wavy solutions; the dashed line represents the localized droplet solution for this value of $\mathscr{V}$.

will arise, but the fluid is unlikely to spread far along the tube. We therefore expect that for large $\mathscr{V}$ (i.e. small δ) the resulting equilibrium state will be well approximated by a localized droplet with a closed contact line, lying predominantly on the outer wall of the tube. Just as axisymmetric wetting collars represent a limit point of the branch of steady unduloids in straight tubes, at which the film thickness tends to zero at some point, so we expect that localized droplet solutions in a weakly curved tube will represent the limit point of a branch of stable wavy solutions, at which wavy contact lines meet at $\phi = \frac{1}{2}\pi$. The confining effect of azimuthal curvature may be overcome by sufficiently strong centreline curvature, however, so that for $\mathscr{V}$ beneath some critical value (i.e. for sufficiently large δ), localized droplet solutions will not exist.

Now a necessary condition for the existence of a localized droplet solution is that $K > 1$. This can be proved by constructing the asymptotic solution for the droplet in the neighbourhood of the intersection of its contact line with $\phi = \frac{1}{2}\pi$. We do so by introducing scaled coordinates (S, Φ) using a small parameter $\hat{\epsilon}$, where $s = -\frac{1}{2}L + \hat{\epsilon}^2 S$, $\phi = \frac{1}{2}\pi + \hat{\epsilon}\Phi$ and $H = \hat{\epsilon}^4 \hat{\mathscr{H}}$. Then (2.10) becomes

$$\hat{\epsilon}^4 \hat{\mathscr{H}} + \hat{\epsilon}^2 \hat{\mathscr{H}}_{\Phi\Phi} + \hat{\mathscr{H}}_{SS} + (1 - \tfrac{1}{2}\hat{\epsilon}^2\Phi^2 + \tfrac{1}{24}\hat{\epsilon}^4\Phi^4 + \ldots) = K. \tag{5.5}$$

The curved droplet boundary will be locally parabolic, given by the curve $\Phi^2 = DS$ in $S \geqslant 0$ for some $D > 0$; applying the boundary conditions $\hat{\mathscr{H}} = 0$, $2\Phi\hat{\mathscr{H}}_\Phi - D\hat{\mathscr{H}}_S = 0$ along this boundary, the leading-order solution of (5.5), i.e. of $\hat{\mathscr{H}}_{SS} = K - 1$, is

$$\hat{\mathscr{H}}(\Phi, S) \sim \tfrac{1}{2}(K-1)\left[S - (\Phi^2/D)\right]^2, \qquad 0 \leqslant S \leqslant \Phi^2/D, \tag{5.6}$$

and so $\hat{\mathscr{H}} > 0$ within the droplet requires $K > 1$.

The critical value of $\mathscr{V}$ beneath which no droplet solutions exist is therefore $\mathscr{V}_1$ (see figure 8). For wavy solutions with $\mathscr{V} < \mathscr{V}_1$ for which $K < 1$, the effects of centreline

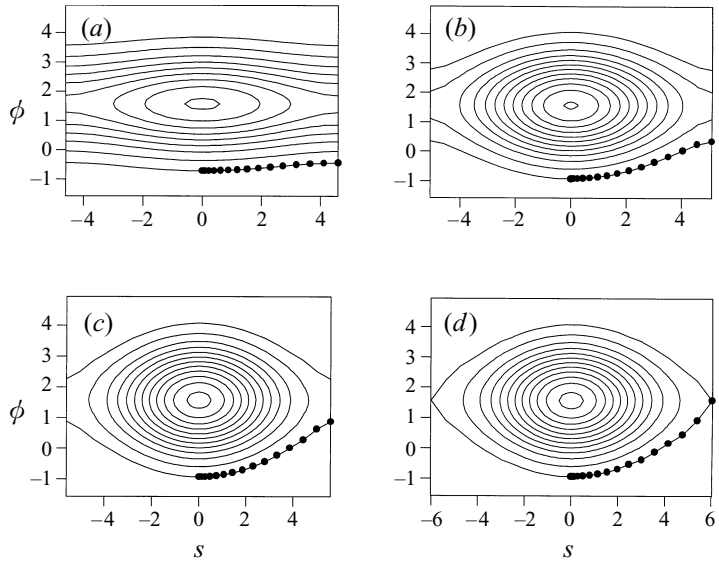

FIGURE 13. Contours of H for $\mathscr{V} = 8$, $N = 16$ and (*a*) $L = 9.2$, (*b*) $L = 10.2$, (*c*) $L = 11.2$ and (*d*) $L = 12.03$. The bullets show the location of the grid points along the contact line. Contour values are $H = 0, 0.1, 0.3, \ldots$ where appropriate.

curvature demand that the fluid spread along the tube wall to the boundaries of the domain, and either wavy or uniform-lobe solutions exist. For $\mathscr{V} > \mathscr{V}_1$, however, as the wavy solutions grow in amplitude with increasing L, they approach a limit point at which the contact lines meet at $s = \pm\frac{1}{2}L$, corresponding to the formation of a drop. Bifurcation diagrams for the case $\mathscr{V} = 8$ (figure 12) illustrate such a transition: the uniform lobe loses stability to a stable wavy lobe at $L \approx 9.156$; the post-critical wavy-lobe solution at $L = 9.2$ is shown in figure 13(*a*); the amplitude of the wavy lobe grows rapidly (e.g. figures 13*b* and 13*c* for which $L = 10.2$ and $L = 11.2$) until $L \approx 12.03$ (figure 13*d*), where the contact lines meet at $\phi = \frac{1}{2}\pi$ and the topology of the solution changes abruptly. For larger L the solution is unchanged (this is represented by a dashed line on figure 12) since increasing the length of dry wall either side of the droplet will not change the solution's amplitude or pressure.

This example was taken from a region of parameter space in which it was necessary to employ a non-uniformly spaced grid (shown with bullets in figure 13) in order to suppress numerical instabilities. The maximum reliable resolution achievable for these parameter values was $N = 16$ (i.e. 32 unknowns). An unfortunate consequence of this was the loss of resolution at $s = \pm\frac{1}{2}L$. Although all the eigenfunctions in (5.1) satisfy periodic boundary conditions at $s = \pm\frac{1}{2}L$, the discretized boundary fails to capture what would be a narrow neck akin to the structure in figure 10(*d*). The neck shares the scaling used in (5.5), so that if the neck width (in ϕ) is $O(\hat{\epsilon})$, its length (in s) is $O(\hat{\epsilon}^2)$. Thus in figure 12, when the domain length L is $O(\hat{\epsilon}^2)$ shorter than the length $\mathscr{L}$, say, of the droplet (indicated with a bullet), the pressure perturbation is $O(\hat{\epsilon}^2) = O(\mathscr{L} - L)$ (from (5.5)) but the amplitude perturbation is $O(\hat{\epsilon}) = O(\mathscr{L} - L)^{1/2}$, explaining the linear and quadratic shape of the wavy solution branches in figures 12(*a*) and 12(*b*) respectively at the bifurcation point. The short lengthscale of the neck as $\hat{\epsilon} \to 0$ represents a challenge to any discrete representation of the solution, which the present method fails to meet. An attempt was made to compute the

droplet solutions directly using Newton's method in polar coordinates centred on the mid-point of the droplet; in this case the eigenfunction expansion in (5.1) is of the form $\sum_{m=0}^{\infty} a_m J_{2m}(r) \cos 2m\theta$. Since Bessel functions decay rapidly with m for fixed r, severe ill-conditioning made it impossible (using orthogonality conditions) to estimate the coefficients a_m beyond the first few for a solution such as that in figure 13(*d*), preventing the scheme from converging to any sensible solution. However, since quantitatively similar results to those in figure 11 could be achieved in a Cartesian geometry with smaller N (e.g. with $N = 10$ the length of the blob with $V = 8$ was approximately 12.14, only 1% different from 12.03 in figure 13*d*), it was judged that these results provide a reasonable approximation of the bifurcation structure in this regime of parameter space, even though some details of the solutions are not fully resolved.

A set of such points at which the wavy solutions (computed using grids as in figure 13) become localized droplets is plotted as curve D on figure 8. (A conservative estimate of the error in the location of this curve can be made by assuming the error in L for fixed $\mathscr{V}$ is bounded above by the largest grid spacing in figure 13*d*; this yields a relative error in L of about 5%.) The curve joins with the line $K = 1$ near $L \approx 13.75$, and asymptotes towards NC_1 as $\mathscr{V}$ becomes large. The amplitude and pressure of the droplet solutions along D are shown with a dashed line in figure 11. As $\mathscr{V}$ increases through $\mathscr{V}_1$, and the solution in figure 10(*d*) loses its arms, K rises smoothly through 1 (figure 11*a*); the drop width (in ϕ) grows slowly beyond the bifurcation point (figure 11*b*), while its length (in s) falls slowly (figure 8). The droplets always have a large aspect ratio, however (figure 13*d*).

6. Discussion

Weak centerline curvature (or equivalently a weak transverse gravitational field) has been shown to have a profound effect on the equilibrium distribution of a thin liquid layer lining the interior of a tube. Draining flows are generated that cause the formation of structures centred on the tube's outer wall, either axially uniform lobes, or wavy lobes or localized droplets. These equilibria, which have been computed assuming that the fluid wets the wall with zero contact angle, are governed by a forced Helmholtz equation (2.10): although this PDE is linear, the nonlinear boundary conditions associated with the free contact line (2.12) allow for multiple steady solutions. The regions of $(L, \mathscr{V})$-parameter space in which each class of solution arise are presented in figure 8. In long tubes there can be hysteresis in transitions between wavy and axially uniform solutions (shown on bifurcation diagrams in figures 9 and 11); the stable wavy solutions in this case generally have a solitary structure (e.g. figure 10*c*, *d*). Multiple steady solutions can also arise at large $\mathscr{V}$ (i.e. for larger fluid volumes or for weaker centerline curvature), where droplet and wavy solutions can coexist (e.g. figure 11). In comparison to straight tubes, centreline curvature suppresses capillary instabilities of thin films (see §4.1), but by breaking the symmetry of the system the bifurcation structure is enriched. Over those regions of the tube wall that are not wetted by equilibrium solutions, there is a slowly draining, vanishingly thin fluid layer (figures 3–5). In practice, intermolecular forces will ultimately determine its fate: if they are stabilizing, the draining will stop once the fluid layer reaches a critical thickness (Reisfeld & Bankoff 1992), in which case the equilibrium solutions computed here will remain valid 'outer' approximations; if the forces are destabilizing, however, the liquid lining will rupture, presumably where the film is thinnest, and new equilibria will arise which have non-zero contact angles

at their contact lines. In the latter case some of the fluid will be trapped in satellite structures on the inner wall or between larger localized droplets on the outer wall. Stability boundaries analogous to those in figure 8 will be significantly affected by such non-wetting effects.

For $(L, \mathscr{V})$-values to the right of the curve D in figure 8, an initially uniform film is predicted to drain ultimately into a localized droplet with volume $\mathscr{V}$ (or, beyond NC_2, say, a wavy lobe with wavelength $\frac{1}{2}L$ may possibly be reached). It would be valuable to compute the corresponding unsteady, two-dimensional draining flow using (2.8) with $\kappa = 1$, because (i) it would reveal the possible transient satellite structures that develop between adjacent droplets and the associated non-planar large-time capillary wave trains (cf. figure 5) adjacent to the droplet's contact line, (ii) it would provide an independent means of computing the localized droplet solutions along curve D in figure 8, and (iii) it would allow comparison between the predictions of the present static stability results (which considers solutions that in principle take an infinite time to develop) and a fully dynamic calculation. A study of long distributed systems that are not tightly constrained by periodic boundary conditions at each end of the tube would also be of interest, since there is the potential for both localized droplets and wavy, solitary solutions in a very long domain to have an irregular distribution along the tube, raising intriguing questions about the pattern-forming properties of this system; energy methods based on spinodal decomposition (Appendix A; Mitlin 1993) may prove valuable in this regard. The author is presently unaware of any published experimental data with which to test these ideas.

A major aim of this work is to help develop an understanding of the factors controlling the liquid-lining distribution in a pulmonary airway bifurcation. Key conclusions from the present study are that a thin liquid lining in an airway with a non-uniformly curved wall will experience a pressure gradient driving a draining flow: even if curvature gradients are weak and the airway short, the flow is felt as a singular perturbation making some draining inevitable, although the rate of drainage may be slow. If an individual airway is sufficiently long (and the effects of gravity can be neglected), axially varying capillary instabilities may develop, provided transverse curvature gradients are sufficiently weak; typically, the mean length of an airway is roughly 7 radii (see, for example, Grotberg 1994), which is close to the critical length $4\pi/\sqrt{3} \approx 7.255$ (the vertical dotted line in figure 8) beyond which wavy equilibria arise. The present theory could in principle be extended to determine the possible liquid-lining equilibria (if they exist) in an accurate morphological model of a bifurcation. Steps in this direction could be taken by considering tubes with non-circular cross-section (for draining flows in a polygonal capillary see Wong *et al.* 1995, for example), tubes with non-uniform centreline curvature and torsion (e.g. at a bend or twist in a pipe), and tubes with tapering cross-section. The latter effect, in particular, will drive axial flows (Halpern, Jensen & Grotberg 1996). Such flows are likely to have significant interactions with capillary instabilities, and careful treatment of moving contact lines may be necessary.

The neglect of gravity in the preceding discussion was a significant assumption. The relative importance of draining flows driven by gravity to those driven by centreline curvature is represented by the parameter

$$\mathscr{B} = \frac{B}{\delta} = \frac{\rho a^2 g}{\sigma \delta} \tag{6.1}$$

(see §2.1). In the terminal bronchioles of the lung, Kamm & Schroter (1989) estimated $B \approx 0.03$. In larger airways, gravity may therefore be the dominant cause of draining:

however, provided B is not too large, and the airways are suitably oriented, the present theory remains applicable. In tilted tubes, the axially uniform lobes represent the solution for unidirectional flow. Curvature effects are likely to be of greater significance in the smallest airways, in conditions of weak buoyancy (i.e. under liquid ventilation or microgravity), in conditions of elevated surface tension (perhaps associated with surfactant deficiency) and in locations of highly non-uniform wall curvature, such as at the apex of a bifurcation.

It is also helpful to consider the effect of weak wall-curvature gradients on thick fluid layers (as might arise in diseased lungs), because of the increased dangers of airway closure in this case. Thin liquid layers feel the effects of non-uniform wall curvature very strongly, so much so that some part of the inner wall of the tube is always left effectively dry. For thicker layers, these effects will be less dramatic, and it should be possible for the inner wall to remain wet for sufficiently large fluid volumes. A simple example helps to demonstrate these ideas. In a straight tube of radius a, a meniscus of fluid wetting the tube wall with zero contact angle exists provided the fluid volume exceeds $\frac{2}{3}\pi a^3$ (Everett & Haynes 1972). The solution with minimum volume has two hemispherical interfaces that touch along the tube axis, and two parallel, circular contact lines a distance $2a$ apart. A similar solution exists in a tube with uniform centreline curvature a/δ, whereby the two hemispherical interfaces touch, but not along the tube centreline, and the contact lines are circles lying in planes that intersect at the centre of centreline curvature. In this case, the minimum fluid volume is given by

$$\frac{V_{min}}{\pi a^3} = \frac{2}{\delta}\sin^{-1}\delta - \tfrac{4}{3} \sim \tfrac{2}{3} + \tfrac{1}{3}\delta^2 + O(\delta^4) \tag{6.2}$$

as $\delta \to 0$. The distance along the tube centreline between the planes of each contact line is then $a(2 + \frac{1}{3}\delta^2 + O(\delta^4))$. Thus the tube length and fluid volume necessary for the existence of a meniscus are larger than in the straight-tube case, so in this sense centreline curvature has a weak stabilizing effect on meniscus formation and airway closure. Since the fluid interface of a meniscus is close to the wall only along contact lines, centreline curvature has only a weak overall effect, appearing as a regular perturbation at $O(\delta^2)$, instead of a singular perturbation at $O(\delta)$, as is the case for a thin film.

The analogy between the effects on a thin film of weak centreline curvature and a weak gravitational field will break down once δ and ϵ are no longer small. Studies of how thicker films respond to stronger gravity, particularly in the presence of an axial flow, would be relevant to core–annular flows in which a lubricated oil core rises to the top of a horizontal pipe, displacing the lubricating water layer around it (see, for example, Joseph & Renardy 1993). Thin-film flows driven by the combined effects of strong curvature gradients and gravity can be treated using the evolution equation of Roy *et al.* (1996); their computations of the curvature-driven flow of a thin film on the exterior of a tightly curved torus show strong similarities with the draining flows in §3. A further potential application of these draining calculations is to the related squeeze-film problem encountered in the pleural space, in which the buoyant lung rises to the top of the pleural cavity, and fluid drains down around it (see, for example, Grotberg 1994). The present results may also be relevant to the distribution of the thin mucus layer lining the eustachian tubes, which are potentially susceptible to both gravitational and curvature-driven forcing.

The airway liquid lining in a healthy lung is covered with a surfactant monolayer, one purpose of which is to stabilize the interface against capillary instabilities (e.g.

Otis *et al.* 1993; Halpern & Grotberg 1993). In the delivery of artificial surfactant to the surfactant-deficient lung of a severely premature infant, an exogenous monolayer spreads along an airway under the action of surface-tension gradients. The modelling of such flows has typically assumed that the airway is a straight cylinder and the liquid lining is azimuthally uniform (e.g. Jensen & Grotberg 1992; Espinosa *et al.* 1993 and references therein). In a weakly curved airway two competing effects will influence the monolayer's progress. First, if the liquid lining is distributed uniformly around the tube, the surfactant will advance quicker along the inner wall (I, figure 1) since it has less far to travel than on the outer wall (O), an effect contained in (2.6); at the leading edge of a spreading monolayer, the surfactant concentration will therefore be $O(\delta)$ larger on I than on O. Second, the surface-tension-driven flow induced by centreline curvature causes the liquid lining to drain to the tube's outer wall (see §3), and since the monolayer travels quicker over deeper fluid it will spread faster along this wall, provided the fluid forms a continuous lobe; the monolayer concentration will then be larger on O than on I by an $O(1)$ amount. Of these two opposite effects, the second is likely to be substantially stronger in general. Thus readjustment of fluid under wall-curvature gradients will therefore have important implications for surfactant transport in the lung, particularly in the neighbourhood of an airway bifurcation.

Appendix A. Energetics

Consider solutions of (2.8) in a domain of fixed length L, of fixed volume V, where

$$V = \langle h \rangle \equiv 2 \int_{-L/2}^{L/2} \mathrm{d}s \int_{-\pi/2}^{\pi/2} \mathrm{d}\phi \; h(s, \phi, t). \tag{A 1}$$

We can define an energy $E = \left\langle -(1 + \delta \sin\phi)h - \frac{1}{2}\epsilon h^2 + \frac{1}{2}\epsilon |\hat{\nabla} h|^2 \right\rangle$. Solutions for which E is stationary under variations in h, subject to the constraint $V =$ constant, satisfy $\delta(E - \hat{p}V)/\delta h = 0$ for some Lagrange multiplier $\hat{p}$. It follows that $\hat{p}$ is exactly the pressure p, given by (2.4). Equation (2.8) with $\kappa = 1$ can then be written in a standard form (e.g. Mitlin 1993)

$$h_t = \hat{\nabla} \cdot \left(\tfrac{1}{3} h^3 \hat{\nabla} \frac{\delta E}{\delta h} \right). \tag{A 2}$$

For static solutions, either $h = 0$ or $p \equiv \delta E/\delta h$ is uniform. A contact-line condition (that the fluid wets the wall with zero contact angle) is required to determine these solutions fully; this yields (2.10)–(2.15). Multiplying (A 2) through by $\delta E/\delta h$, integrating over one wavelength, applying the divergence theorem and the no-flux conditions around the perimeter of the domain, it follows that

$$\frac{\mathrm{d}E}{\mathrm{d}t} = -\left\langle \tfrac{1}{3} h^3 \left| \nabla \frac{\delta E}{\delta h} \right|^2 \right\rangle \leqslant 0. \tag{A 3}$$

Thus the energy E decreases as the flow evolves, and for static solutions $\mathrm{d}E/\mathrm{d}t = 0$. The system approaches one of the stable equilibrium states as $t \to \infty$.

Appendix B. Large-time asymptotics: the capillary wave train

In region (II) the leading-order problem is given by (3.12) and (3.13). By stating the problem in this non-standard way a solution can be obtained directly. In this

problem solutions cannot be approximated by functions with simple power-law time dependence; they have a more complex unsteady behaviour that can be captured by allowing time to parameterize solutions of (3.12).

Far upstream, $G \sim 1 + a_1 \exp\left[\frac{1}{2}3^{1/3}\xi\right] \cos\left(\frac{1}{2}3^{5/6}(\xi - a_2)\right)$ as $\xi \to -\infty$ for constants a_1 and a_2, a decaying wave corresponding to those in figure 5. Far downstream, solutions of (3.12) develop large nonlinear relaxation oscillations which increase rapidly in amplitude and wavelength as ξ increases (Wilson & Jones 1983). These can be approximated using matched asymptotic expansions. The outer solution for oscillation n, say, has $G \gg 1$ and is governed at leading order by $0 = 1 + G_{\xi\xi\xi\xi}$, so that

$$G \sim \tfrac{1}{2}C_n(\xi - \xi_n)^2 - \tfrac{1}{6}(\xi - \xi_n)^3, \qquad \xi_n < \xi < \xi_{n+1} \equiv \xi_n + 3C_n, \tag{B 1}$$

for some constant $C_n > 0$. This solution satisfies $G = G_\xi = 0$ and $G_{\xi\xi} = C_n$ at $\xi = \xi_n$, $G = G^{(n)}_{\max} = \frac{2}{3}C_n^3$ at $\xi = \xi_n + 2C_n$ and $G = 0$, $G_\xi = -\frac{3}{2}C_n^2$ at $\xi = \xi_{n+1}$. Oscillations n and $n+1$ are related by the inner solution which applies over a very short lengthscale at ξ_{n+1}, for which $G \ll 1$ and

$$1 = G^3 G_{\xi\xi\xi\xi}, \qquad G \sim -\beta_1\xi \quad \text{as} \quad \xi \to -\infty, \qquad G \sim \tfrac{1}{2}\beta_2\xi^2 \quad \text{as} \quad \xi \to \infty, \tag{B 2}$$

where $\beta_1 = \frac{3}{2}C_n^2$ and $\beta_2 = C_{n+1}$. The inner problem is related directly to the canonical problem (3.5) by scaling G by β_1^{-3}, ξ by β_1^{-4} and setting $\beta_2 = \beta_1^5\mathscr{C}$. Thus

$$G^{(n+1)}_{min} \sim \frac{2^3\mathscr{M}}{3^3C_n^6} = \mathscr{M}\left(\frac{\mathscr{C}}{C_{n+1}}\right)^{3/5} \qquad C_{n+1} = \frac{3^5\mathscr{C}}{2^5}C_n^{10} \tag{B 3}$$

as $n \to \infty$, and the lengthscale of the inner region is $O(C_n^{-8}) \sim O(C_{n+1}^{-4/5})$.

We can now match the upstream end of oscillation $n+1$ at ξ_{n+1} to the filling lobe solution in region (III), by taking $C_{n+1} = \Lambda \sim T^{1/6}$. Fixing C_{n+1} as a function of T yields $C_n \sim T^{1/60}$, $C_{n-1} \sim T^{1/600}, \ldots$ and hence the full asymptotic solution for G. The film is thinnest over a short region equivalent to the inner region at ξ_{n+1}, so that

$$h_{min} \sim \left[\frac{S_0^6\mathscr{M}^5\mathscr{C}^3\cos^2\alpha_0}{C^2(K_0 - \sin\alpha_0)^3T^3}\right]^{1/5} \tag{B 4}$$

(as in figures 4 and 5) and the lengthscale of the constriction is $O(T^{-3/10})$, yielding region (IIa). The local maximum in film height just upstream of the constriction (equivalent to the maximum of oscillation n) has $h \sim T^{-9/20}$ (figure 5) over a lengthscale $O(T^{-3/20})$ (region IIb, say). Continuing further upstream, the next minimum has $h \sim T^{-51/100}$ (region IIc) over a lengthscale $O(T^{-9/50})$, the next maximum has $h \sim T^{-99/200}$ over a lengthscale $O(T^{-33/200})$ (region IId), and so on. These quantities are in practice indistinguishable from $h \sim T^{-1/2}$ and the $O(T^{-1/6})$ lengthscale (region II) for all but the very largest times, so only the capillary wave immediately upstream of the constriction is likely to exhibit its asymptotic scalings as $T \to \infty$.

REFERENCES

Bretherton, F. P. 1961 The motion of long bubbles in tubes. *J. Fluid Mech.* **10**, 166–188.

Brown, R. A. & Scriven, L. E. 1980 On the multiple equilibrium shapes and stability of an interface pinned on a slot. *J. Colloid Interface Sci.* **78**, 528–542.

Davis, S. H. 1980 Moving contact lines and rivulet instabilities. Part 1. The static rivulet. *J. Fluid Mech.* **98**, 225–242

Espinosa, F. F., Shapiro, A. H., Fredberg, J. J. & Kamm, R. D. 1993 Spreading of exogenous surfactant in an airway. *J. Appl. Physiol.* **75**, 2028–2039.

Everett, D. H. & Haynes, J. M. 1972 Model studies of capillary condensation: I. Cylindrical pore model with zero contact angle. *J. Colloid Interface Sci.* **38**, 125–137.

Frankel, S. P. & Mysels, K. J. 1962 On the 'dimpling' during the approach of two interfaces. *J. Phys. Chem.* **66**, 190–191.

Gauglitz, P. A. & Radke, C. J. 1988 An extended evolution equation for liquid film breakup in cylindrical capillaries. *Chem. Engng Sci.* **43**, 1457–1465.

Goren, S. L. 1962 The instability of an annular thread of fluid. *J. Fluid Mech.* **12**, 309–319.

Grotberg, J. B. 1994 Pulmonary flow and transport phenomena. *Ann. Rev. Fluid Mech.* **26**, 529–571.

Halpern, D. & Grotberg, J. B. 1993 Surfactant effects on fluid-elastic instabilities of liquid-lined flexible tubes: a model of airway closure. *Trans. ASME J. Biomech. Engng* **115**, 271–277; and Corrigendum **116**, 133.

Halpern, D., Jensen, O. E. & Grotberg, J. B. 1996 A theoretical study of surfactant spreading in a simple lung model (preprint).

Hammond, P. S. 1983 Nonlinear adjustment of a thin annular film of viscous fluid surrounding a thread of another within a circular cylindrical pipe. *J. Fluid Mech.* **137**, 363–384.

Higgins B. G. & Brown, R. A. 1984 Multiple equilibrium shapes of partially constrained menisci: a quasi-static mechanism for instability of a coating bead. *Chem. Engng Sci.* **39**, 1339–1345.

Jensen, O. E. & Grotberg, J. B. 1992 Insoluble surfactant spreading on a thin viscous film: shock evolution and film rupture. *J. Fluid Mech.* **240**, 259–288.

Johnson, M. Kamm, R. D., Ho, L. W., Shapiro, A. & Pedley, T. J. 1991 The nonlinear growth of surface-tension-driven instabilities of a thin annular film. *J. Fluid Mech.* **233**, 141–156.

Jones, A. F. & Wilson, S. D. R. 1978 The film drainage problem in droplet coalescence. *J. Fluid Mech.* **87**, 263–288.

Joseph, D. D. & Renardy, Y. Y. 1993 *Fundamentals of Two-Fluid Dynamics. Part II: Lubricated Transport, Drops and Miscible Liquids.* Springer.

Kamm, R. D. & Schroter, R. C. 1989 Is airway closure caused by a liquid film instability? *Respir. Physiol.* **75**, 141–156.

Langbein, D. 1990 The shape and stability of liquid menisci at solid edges. *J. Fluid Mech.* **213**, 251–265.

Macklem, P. T., Proctor, D. F. & Hogg, J. C. 1970 The stability of peripheral airways. *Respir. Physiol.* **8**, 191–203.

Michael, D. H. 1981 Meniscus stability. *Ann. Rev. Fluid Mech.* **13**, 189–215.

Mitlin, V. S. 1993 Dewetting of solid surface: analogy with spinodal decomposition. *J. Colloid Interface Sci.* **156**, 491–497.

Nayfeh, A. H. 1970 Nonlinear stability of a liquid jet. *Phys. Fluids* **13**, 841–847.

Newhouse, L. A. & Pozrikidis, C. 1992 The capillary instability of annular layers and liquid threads. *J. Fluid Mech.* **242**, 193–209.

Olbricht, W. L. 1996 Pore-scale prototypes of multiphase flow in porous media. *Ann. Rev. Fluid Mech.* **28**, 187–213.

Otis, D. R., Johnson, M., Pedley, T. J. & Kamm, R. D. 1992 The role of pulmonary surfactant in airway closure: a computational study. *J. Appl. Physiol.* **75**, 1323–1333.

Plateau, J. 1873 *Statique Expérimentale et Théorique des Liquides Soumis aux Seules Forces Moléculaires.* Gauthier–Villars.

Princen, H. M. 1963 Shape of a fluid drop at a liquid-liquid interface. *J. Colloid Sci.* **18**, 178.

Rayleigh, Lord 1879 On the instability of jets. *Proc. R. Soc. Lond.* A **10**, 4–13.

Reisfeld, B. & Bankoff, S. G. 1992 Non-isothermal flow of a liquid film on a horizontal cylinder. *J. Fluid Mech.* **236**, 167–196.

Roy, R. V., Roberts, A. J. & Simpson, M. E. 1996 A lubrication model of coating flows over a curved substrate in space. *J. Fluid Mech.* (submitted).

Sáez, A. E. & Carbonnell, R. G. 1987 The equilibrium shape and stability of menisci formed between two touching cylinders. *J. Fluid Mech.* **176**, 357–378.

Schwartz, L. W., Princen, H. M. & Kiss, A. D. 1986 On the motion of bubbles in capillary tubes. *J. Fluid Mech.* **172**, 259–275.

Schwartz, L. W. & Weidner, D. E. 1995 Modeling of coating flows on curved surfaces. *J. Engng Maths* **29**, 91–103.

Tuck, E. O. & Schwartz, L. W. 1991 Thin static drops with a free attachment boundary. *J. Fluid Mech.* **223**, 313–324.

Ungar, L. H. & Brown, R. A. 1982 The dependence of the shape and stability of captive rotating drops on multiple parameters. *Phil. Trans. R. Soc. Lond.* A **306**, 347–370.

Wilson, S. D. R. & Jones, A. F. 1983 The entry of a falling film into a pool and the air-entrainment problem. *J. Fluid Mech.* **128**, 219–230.

Wong, H., Radke, C. J. & Morris S. 1995 Motion of long bubbles in polygonal capillaries. Part 1. *J. Fluid Mech.* **292**, 71–94.

Wu, R. & Weinbaum, S. 1982 On the development of fluid trapping beneath deformable fluid-cell membranes. *J. Fluid Mech.* **121**, 315–343.

Yiantsios, S. G. & Davis, R. H. 1990 On the buoyancy-driven motion of a drop towards a rigid surface or a deformable interface. *J. Fluid Mech.* **217**, 547–573.

Yiantsios, S. G. & Higgins, B. G. 1989 Rayleigh-Taylor instability in thin viscous films. *Phys. Fluids* A **1**, 1484–1501.